https://ntrs.nasa.gov/search.jsp?R=19730017173 2020-03-11T19:10:53+00:00Z

25900

NASA TECHNICAL NOTE

N73-25900
NASA TN D-7316

NASA TN D-7316

CASE FILE COPY

# AN ANALYSIS OF ATMOSPHERIC ENTRY TRAJECTORIES FOR MANNED AND UNMANNED MISSIONS TO THE PLANET VENUS

*by Mark K. Craig and Ralph G. Gonzalez*

*Manned Spacecraft Center*
*Houston, Texas 77058*

NATIONAL AERONAUTICS AND SPACE ADMINISTRATION • WASHINGTON, D. C. • JUNE 1973

| 1. Report No. | 2. Government Accession No. | 3. Recipient's Catalog No. |
|---|---|---|
| NASA TN D-7316 | | |

| 4. Title and Subtitle | 5. Report Date |
|---|---|
| AN ANALYSIS OF ATMOSPHERIC ENTRY TRAJECTORIES FOR MANNED AND UNMANNED MISSIONS TO THE PLANET VENUS | June 1973 |
| | 6. Performing Organization Code |

| 7. Author(s) | 8. Performing Organization Report No. |
|---|---|
| Mark K. Craig and Ralph G. Gonzalez, MSC | MSC S-212 |
| | 10. Work Unit No. 976-30-90-01-72 |

| 9. Performing Organization Name and Address | 11. Contract or Grant No. |
|---|---|
| Manned Spacecraft Center<br>Houston, Texas 77058 | |
| | 13. Type of Report and Period Covered: Technical Note |

| 12. Sponsoring Agency Name and Address | 14. Sponsoring Agency Code |
|---|---|
| National Aeronautics and Space Administration<br>Washington, D.C. 20546 | |

15. Supplementary Notes

16. Abstract

A unified atmospheric density model is presented for the planet Venus, and this model is compatible with Russian and American data obtained during the 1967 Venus launch opportunity. Trajectory characteristics involved in atmospheric entry are discussed with reference to roll-control modulation and entry corridor. Subsequent to a trajectory-oriented discussion of potential Venus mission characteristics, a parametric analysis of manned and unmanned vehicle entry trajectories into the Venusian atmosphere is presented. A sensitivity analysis with reference to atmospheric density deviations is included to show the dependence of corridor depth on the atmospheric density profile.

| 17. Key Words (Suggested by Author(s)) | 18. Distribution Statement |
|---|---|
| *Interplanetary Spacecraft<br>*Venus<br>*Planetary Entry<br>*Entry Trajectories | |

| 19. Security Classif. (of this report) | 20. Security Classif. (of this page) | 21. No. of Pages | 22. Price* |
|---|---|---|---|
| None | None | 44 | $3.00 |

* For sale by the National Technical Information Service, Springfield, Virginia 22151

CONTENTS


| Section | Page |
|---|---|
| SUMMARY | 1 |
| INTRODUCTION | 1 |
| SYMBOLS | 2 |
| ATMOSPHERIC AND GEOPHYSICAL PROPERTIES OF VENUS | 3 |
| ATMOSPHERIC ENTRY MISSION CHARACTERISTICS | 5 |
| Roll-Modulation Trajectory Control | 5 |
| Entry Corridor | 6 |
| Manned Missions | 6 |
| Unmanned Missions | 7 |
| Baseline Spacecraft and Trajectory Parameters | 9 |
| RESULTS AND DISCUSSION | 9 |
| Manned Entry | 9 |
| Unmanned-Probe Entry | 21 |
| CONCLUDING REMARKS | 32 |
| REFERENCES | 34 |

FIGURES


| Figure | | Page |
|---|---|---|
| 1 | Venus atmospheric-density profile | 5 |
| 2 | Venus aerobraking maneuver | |
| | (a) Trajectory near the overshoot boundary | 7 |
| | (b) Trajectory near the undershoot boundary | 7 |
| | (c) Representative trajectory profile near the overshoot boundary | 8 |
| | (d) Representative trajectory profile near the undershoot boundary | 8 |
| 3 | Undershoot and overshoot boundary vacuum periapsis radii as a function of spacecraft ballistic parameter | |
| | (a) L/D = 0.25 | 10 |
| | (b) L/D = 0.50 | 10 |
| | (c) L/D = 1.00 | 10 |
| 4 | Entry-corridor depth as a function of spacecraft ballistic parameter | |
| | (a) L/D = 0.25 | 10 |
| | (b) L/D = 0.50 | 10 |
| | (c) L/D = 1.00 | 10 |
| 5 | Undershoot and overshoot boundary entry-flight-path angles as a function of spacecraft ballistic parameter | |
| | (a) L/D = 0.25 | 11 |
| | (b) L/D = 0.50 | 11 |
| | (c) L/D = 1.00 | 11 |
| 6 | Undershoot boundary maximum dynamic pressure as a function of spacecraft ballistic parameter | |
| | (a) L/D = 0.25 | 12 |
| | (b) L/D = 0.50 | 12 |
| | (c) L/D = 1.00 | 12 |
| 7 | Undershoot boundary pullout altitude and velocity as a function of spacecraft ballistic parameter | |
| | (a) L/D = 0.25 | 12 |
| | (b) L/D = 0.50 | 12 |
| | (c) L/D = 1.00 | 12 |

Figure | Page

8 Overshoot boundary pullout altitude and velocity as a function of spacecraft ballistic parameter

(a) L/D = 0.25 . . . . . 13
(b) L/D = 0.50 . . . . . 13
(c) L/D = 1.00 . . . . . 13

9 Undershoot and overshoot boundary vacuum periapsis radii as a function of entry velocity

(a) L/D = 0.25, $W/C_DA$ = 100 lb/ft$^2$ . . . . . 14
(b) L/D = 0.50 $W/C_DA$ = 100 lb/ft$^2$ . . . . . 14
(c) L/D = 1.00, $W/C_DA$ = 100 lb/ft$^2$ . . . . . 14
(d) L/D = 0.25, $W/C_DA$ = 500 lb/ft$^2$ . . . . . 14
(e) L/D = 0.50, $W/C_DA$ = 500 lb/ft$^2$ . . . . . 14
(f) L/D = 1.00, $W/C_DA$ = 500 lb/ft$^2$ . . . . . 14
(g) L/D = 0.25, $W/C_DA$ = 1000 lb/ft$^2$ . . . . . 15
(h) L/D = 0.50, $W/C_DA$ = 1000 lb/ft$^2$ . . . . . 15
(i) L/D = 1.00, $W/C_DA$ = 1000 lb/ft$^2$ . . . . . 15

10 Entry-corridor depth as a function of entry velocity . . . . . 15

11 Overshoot boundary entry-flight-path angle as a function of entry velocity

(a) L/D = 0.25 . . . . . 15
(b) L/D = 0.50 . . . . . 16
(c) L/D = 1.00 . . . . . 16

12 Undershoot boundary maximum dynamic pressure as a function of entry velocity

(a) L/D = 0.25 . . . . . 16
(b) L/D = 0.50 . . . . . 16
(c) L/D = 1.00 . . . . . 17

13 Undershoot boundary pullout altitude as a function of entry velocity

(a) L/D = 0.25 . . . . . 17
(b) L/D = 0.50 . . . . . 17
(c) L/D = 1.00 . . . . . 18

| Figure | | Page |
|---|---|---|
| 14 | Overshoot boundary pullout altitude as a function of entry velocity | |
| | (a) L/D = 0.25 | 18 |
| | (b) L/D = 0.50 | 18 |
| | (c) L/D = 1.00 | 18 |
| 15 | Entry-corridor depth as a function of spacecraft trim lift-to-drag ratio | 19 |
| 16 | Overshoot boundary entry flight path angle as a function of spacecraft trim lift-to-drag ratio | |
| | (a) $V_E$ = 36 000 ft/sec | 19 |
| | (b) $V_E$ = 48 000 ft/sec | 19 |
| 17 | Undershoot boundary maximum dynamic pressure as a function of spacecraft trim lift-to-drag ratio | |
| | (a) $V_E$ = 36 000 ft/sec | 19 |
| | (b) $V_E$ = 48 000 ft/sec | 19 |
| 18 | Undershoot boundary pullout altitude as a function of spacecraft trim lift-to-drag ratio | |
| | (a) $V_E$ = 36 000 ft/sec | 20 |
| | (b) $V_E$ = 48 000 ft/sec | 20 |
| 19 | Overshoot boundary pullout altitude as a function of spacecraft trim lift-to-drag ratio | |
| | (a) $V_E$ = 36 000 ft/sec | 20 |
| | (b) $V_E$ = 48 000 ft/sec | 20 |
| 20 | Entry-corridor depth as a function of entry velocity for ±50 percent atmospheric-density deviation | |
| | (a) L/D = 0.50 | 21 |
| | (b) L/D = 1.00 | 21 |
| 21 | Overshoot boundary entry-flight-path angle as a function of spacecraft ballistic parameter | |
| | (a) L/D = 0 | 22 |
| | (b) L/D = 0.25 | 22 |

Figure | Page

22 Overshoot boundary vacuum periapsis radius as a function of spacecraft ballistic parameter

(a) L/D = 0 . . . . . 22
(b) L/D = 0.25 . . . . . 22

23 Entry-flight-path angle as a function of spacecraft ballistic parameter for the overshoot boundary, the 10.8-n. mi. entry corridor, and the 27-n. mi. entry corridor

(a) L/D = 0, $V_E$ = 36 000 ft/sec . . . . . 22
(b) L/D = 0.25, $V_E$ = 36 000 ft/sec . . . . . 22
(c) L/D = 0, $V_E$ = 48 000 ft/sec . . . . . 23
(d) L/D = 0.25, $V_E$ = 48 000 ft/sec . . . . . 23

24 Maximum Earth load factor as a function of spacecraft ballistic parameter for the overshoot boundary, the 10.8-n. mi. entry corridor, the 27-n. mi. entry corridor, and direct entry

(a) L/D = 0, $V_E$ = 36 000 ft/sec . . . . . 23
(b) L/D = 0.25, $V_E$ = 36 000 ft/sec . . . . . 23
(c) L/D = 0, $V_E$ = 48 000 ft/sec . . . . . 24
(d) L/D = 0.25, $V_E$ = 48 000 ft/sec . . . . . 24

25 Maximum dynamic pressure as a function of spacecraft ballistic parameter for the overshoot boundary, the 10.8-n. mi. entry corridor, the 27-n. mi. entry corridor, and direct entry

(a) L/D = 0, $V_E$ = 36 000 ft/sec . . . . . 24
(b) L/D = 0.25, $V_E$ = 36 000 ft/sec . . . . . 24
(c) L/D = 0, $V_E$ = 48 000 ft/sec . . . . . 25
(d) L/D = 0.25, $V_E$ = 48 000 ft/sec . . . . . 25

26 Overshoot boundary entry-flight-path angle as a function of entry velocity

(a) L/D = 0 . . . . . 25
(b) L/D = 0.25 . . . . . 25

27 Entry-flight-path angle as a function of entry velocity for the overshoot boundary, the 10.8-n. mi. entry corridor, and the 27-n. mi. entry corridor

(a) L/D = 0, $M/C_DA$ = 0.5 slug/ft$^2$ . . . . . 25
(b) L/D = 0.25, $M/C_DA$ = 0.5 slug/ft$^2$ . . . . . 25

| Figure | | Page |
|---|---|---|
| 27 | (c) L/D = 0, $M/C_DA$ = 1.0 slug/ft$^2$ | 26 |
| | (d) L/D = 0.25, $M/C_DA$ = 1.0 slug/ft$^2$ | 26 |
| | (e) L/D = 0, $M/C_DA$ = 1.5 slug/ft$^2$ | 26 |
| | (f) L/D = 0.25, $M/C_DA$ = 1.5 slug/ft$^2$ | 26 |
| | (g) L/D = 0, $M/C_DA$ = 2.0 slug/ft$^2$ | 26 |
| | (h) L/D = 0.25, $M/C_DA$ = 2.0 slug/ft$^2$ | 26 |
| 28 | Maximum Earth load factor as a function of entry velocity for the overshoot boundary, the 10.8-n. mi. entry corridor, and the 27-n. mi. entry corridor | |
| | (a) L/D = 0, $M/C_DA$ = 0.5 slug/ft$^2$ | 27 |
| | (b) L/D = 0.25, $M/C_DA$ = 0.5 slug/ft$^2$ | 27 |
| | (c) L/D = 0, $M/C_DA$ = 1.0 slug/ft$^2$ | 27 |
| | (d) L/D = 0.25, $M/C_DA$ = 1.0 slug/ft$^2$ | 27 |
| | (e) L/D = 0, $M/C_DA$ = 1.5 slug/ft$^2$ | 28 |
| | (f) L/D = 0.25, $M/C_DA$ = 1.5 slug/ft$^2$ | 28 |
| | (g) L/D = 0, $M/C_DA$ = 2.0 slug/ft$^2$ | 28 |
| | (h) L/D = 0.25, $M/C_DA$ = 2.0 slug/ft$^2$ | 28 |
| 29 | Maximum dynamic pressure as a function of entry velocity for the overshoot boundary, the 10.8-n. mi. entry corridor, and the 27-n. mi. entry corridor | |
| | (a) L/D = 0, $M/C_DA$ = 0.5 slug/ft$^2$ | 28 |
| | (b) L/D = 0.25, $M/C_DA$ = 0.5 slug/ft$^2$ | 28 |
| | (c) L/D = 0, $M/C_DA$ = 1.0 slug/ft$^2$ | 29 |
| | (d) L/D = 0.25, $M/C_DA$ = 1.0 slug/ft$^2$ | 29 |
| | (e) L/D = 0, $M/C_DA$ = 1.5 slug/ft$^2$ | 29 |
| | (f) L/D = 0.25, $M/C_DA$ = 1.5 slug/ft$^2$ | 29 |
| | (g) L/D = 0, $M/C_DA$ = 2.0 slug/ft$^2$ | 30 |
| | (h) L/D = 0.25, $M/C_DA$ = 2.0 slug/ft$^2$ | 30 |
| 30 | Entry-from-orbit overshoot boundary flight-path angle as a function of spacecraft ballistic parameter | |
| | (a) L/D = 0 | 30 |
| | (b) L/D = 0.25 | 30 |

Figure Page

31 Entry-from-orbit overshoot boundary vacuum periapsis radius as a function of spacecraft ballistic parameter

(a) L/D = 0 . . . . . 31
(b) L/D = 0.25 . . . . . 31

32 Entry-flight-path angle and velocity as a function of apoapsis retrofire velocity reduction for deorbit from a 200- by 10 000-n. mi. elliptical orbit . . . . . 31

33 Maximum Earth load factor as a function of spacecraft ballistic parameter for entry from a 200- by 10 000-n. mi. elliptical orbit; L/D = 0 . . . . . 31

34 Maximum dynamic pressure as a function of spacecraft ballistic parameter for entry from a 200- by 10 000-n. mi. elliptical orbit

(a) L/D = 0 . . . . . 32
(b) L/D = 0.25 . . . . . 32

# AN ANALYSIS OF ATMOSPHERIC ENTRY TRAJECTORIES FOR MANNED AND UNMANNED MISSIONS TO THE PLANET VENUS

By Mark K. Craig and Ralph G. Gonzalez
Manned Spacecraft Center

## SUMMARY

Data obtained from Venera IV and Mariner V Venus probes were unified into an atmospheric model suitable as a basis for this entry study. The unification was accomplished by reconciling both data sets to a nominal value of the Venusian radius and then constructing a density profile for the portion of the atmosphere encountered during entry.

A parametric analysis was undertaken to evaluate the effects on entry performance of variance in both spacecraft and trajectory characteristics. Spacecraft characteristics were modeled by the selection of a representative range of values of the ballistic parameter and the lift-to-drag ratio. Trajectory characteristics pertinent to the definition of both the guidance and load-constrained entry corridors were examined.

A sensitivity analysis was performed to determine the effects on entry performance of dispersions in the atmospheric density profile.

## INTRODUCTION

A knowledge of the physical loads that the vehicle and its payload will have to endure is important in the design of any space vehicle. Whether the vehicle is manned or unmanned, these loads must be defined accurately and systems tolerance levels must be established and adhered to closely. Because atmospheric entry is responsible for the generation of severe loading conditions, an envelope of entry trajectories must be developed that constrains these loads to a level tolerable to both the vehicle and its payload.

A parametric analysis of atmospheric entry trajectories for both manned and unmanned missions to the planet Venus is presented in this report. The objective of this analysis is to provide trajectory characteristics as a function of normalized vehicle parameters. Such a study represents the basic step in the preliminary definition of spacecraft design by providing specific guideline considerations as to the design-related analysis of planetary-approach guidance requirements, spacecraft aerothermodynamic heat-protection requirements, and overall aeroshell structural design requirements.

Because of its relevance to entry trajectories, a discussion of various planetary-mission profiles that would involve entry into the atmosphere of Venus is included. The entry modes considered are direct entry from hyperbolic approach trajectories for both manned and unmanned reconnaissance missions and controlled entry from orbit for unmanned probes.

Entry trajectories were initiated at an altitude of 182.9 kilometers (600 000 feet) and were generated by the equations of motion of a rigid body in three-dimensional space. The trajectories were both shaped and integrated by the computer program documented in reference 1.

Qualitative background material pertinent to entry-flight-trajectory shaping is included throughout the text. A thorough discussion of a majority of this timely material may be found in references 2 to 4.

## SYMBOLS

| | |
|---|---|
| A | effective vehicle cross sectional area, $ft^2$ |
| $C_D$ | drag coefficient, $\frac{D}{1/2\ \rho\ V^2 A}$ |
| $C_L$ | lift coefficient, $\frac{L}{1/2\ \rho\ V^2 A}$ |
| D | drag force, pounds |
| G | local gravitational acceleration, $ft/sec^2$ |
| g | Earth load factor, 32.2 $ft/sec^2$ |
| h | altitude above Venusian surface, feet |
| L | lift force, pounds |
| M | vehicle mass, slugs |
| $M/C_D A$ | ballistic parameter, $slug/ft^2$ |
| q | dynamic pressure, $lb/ft^2$ |
| R | local distance to planet center, n. mi. |
| V | vehicle velocity with respect to planet center, ft/sec |

| | |
|---|---|
| $\overline{V}$ | $\frac{\text{vehicle velocity}}{\text{local circular velocity}}, \frac{V}{\sqrt{GR}}$ |
| W | vehicle weight, pounds |
| $W/C_DA$ | ballistic parameter, $lb/ft^2$ |
| $\gamma$ | inertial flight-path angle, degrees |
| $\Delta R_p$ | entry corridor depth, n. mi. |
| $\rho$ | atmospheric density, $slug/ft^3$ |
| $\phi$ | vehicle roll angle, degrees |
| $(\dot{})$ | derivative of ( ) with respect to time |

Subscripts:

| | |
|---|---|
| D | drag |
| E | condition at entry altitude |
| L | lift |
| max | maximum |
| p | periapsis condition |
| pt | pullout (pitchover) condition |

## ATMOSPHERIC AND GEOPHYSICAL PROPERTIES OF VENUS

Past analysis of the Venusian environment, based on Earth and flyby spacecraft observations, has yielded a fairly broad field of conjecture as to the characteristics of the atmosphere of Venus (refs. 5 to 7). However, data retrieved from the Soviet spacecraft Venera IV and the American spacecraft Mariner V, both of which encountered Venus in October of 1967, has caused a significant reappraisal of these characteristics. Although specific data-point measurements of atmospheric parameters by the two spacecraft do not coincide, a model atmosphere may be constructed which, for the purposes of entry operations, can be reconciled with both data sources.

The noncoincidence of the data primarily results from differences in the altitude-reference systems of the two spacecraft. Mariner V, in its swingby-mode radio-occultation experiment, referenced the center of the Venusian gravitational field as

datum. However, Venera IV used an onboard radio altimeter to sense its altitude above the local planet surface. For this reason, a comparison of the data is dependent on a value of the radius of Venus.

The atmosphere examined by the Mariner V radio-occultation experiment covers a band 55 kilometers in depth, beginning with signal sensitivity to the neutral atmosphere at a radial distance of 6143 kilometers and ending with excessive defocusing attenuation of the signal at 6088 kilometers (ref. 8). Venera IV data acquisition, initiated at the radio altimeter altitude of 26 kilometers, covers a pressure range of from approximately 735 millibars initially to 18 500 millibars at what was deduced to be the Venusian surface (refs. 9 and 10). This deduction was based on both the integration downward of the barometric equation and the subsequent calculation of the rate of descent of the parachute (ref. 11), each of which resulted in verification of the fact that 26 kilometers had been traversed.

The Venera IV data can be made a function of planetocentric distance rather than altitude above the local planet surface by alining the Venera pressure and temperature profiles with the corresponding Mariner data. Such superposition reveals that the Venera measurements range between the radial distances of 6105 and 6079 kilometers (ref. 8). If the Venera IV measurements do extend to the surface, the radius of Venus must be considered to be approximately 6079 kilometers. This figure is in variance with Earth-based planetary radar measurements that have yielded a Venus radius of 6056 kilometers (ref. 12). A second and independent analysis of the Venusian radius, using radar-range data, has resulted in verification of this figure, with a value of 6053.7 kilometers (ref. 13). The accuracy of both this radius value and the analysis of Mariner V atmospheric data indicate that Venera IV did indeed sample a 26-kilometer interval of the Venusian atmosphere but that it traversed this distance between the approximate altitudes of 51 and 25 kilometers. Apparently, Venera IV measured a point 25 kilometers above the mean surface radius as zero reference altitude. Therefore, the addition of 25 kilometers to the Venera altitude scale reconciles, to a satisfactory degree, the model atmospheres constructed from the Venera IV and Mariner V data.

A density profile was constructed from the surface of the planet to an altitude of 70 kilometers using the Venera IV and Mariner V unified data presented in reference 8. The profile was extended to the entry altitude of 182.9 kilometers (600 000 feet) by assuming a constant density scale height of approximately 5.56 kilometers (fig. 1).

The planet was considered to be spherical and nonrotating for the purposes of the trajectory analysis. The assumption that Venus has no axial rotation is valid in light of its estimated period of approximately 250 Earth days (ref. 6). The Venusian gravitational parameter was taken to be 324 682 $km^3/sec^2$ (11 465 968 $ft^3/sec^2$) (ref. 6). In all instances, the atmosphere was assumed to be static.

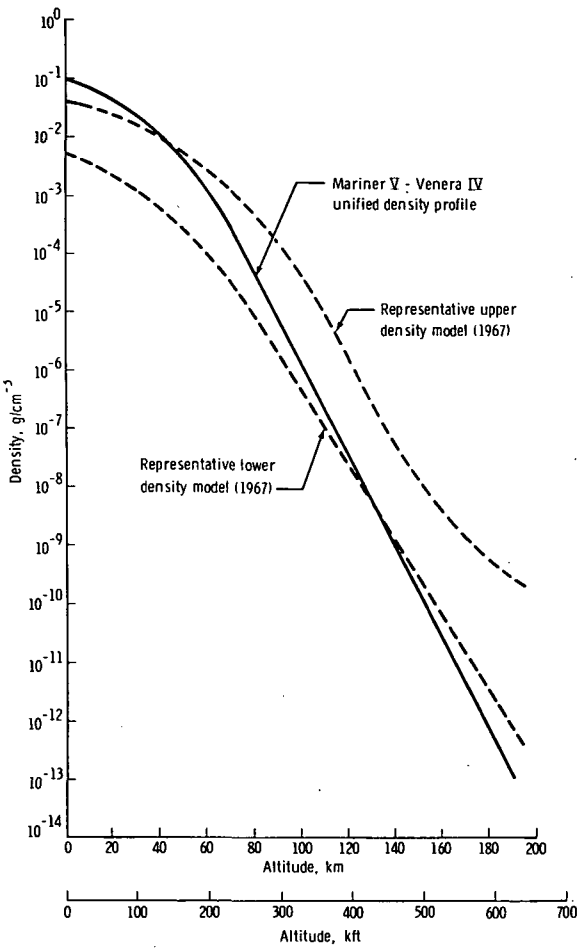


Figure 1.- Venus atmospheric-density profile.

# ATMOSPHERIC ENTRY MISSION CHARACTERISTICS

A knowledge of entry mission characteristics and their associated implications involving spacecraft structural and guidance capabilities is essential to an analysis of entry trajectories. Material is presented in this section defining two concepts that are fundamental to a meaningful description of entry trajectories: roll-modulation trajectory control and entry corridor. The characteristics of feasible manned and unmanned missions to Venus are defined in terms of these concepts.

## Roll-Modulation Trajectory Control

A spacecraft design parameter of primary importance is the vehicle aerodynamic lift capability. Vehicles not capable of lift, usually exploratory probes, are restricted to ballistic entry trajectories. However, lifting vehicles are capable of performing maneuverable atmospheric descents and skipout-into-orbital-capture operations. Spacecraft maneuverability in lifting vehicles is achieved by selective modulation of the lift vector about the vehicle roll axis. This lift-force modulation allows constant-altitude flight during entry, thus providing an efficient means of dissipating vehicle kinetic energy within the framework of the overall mission objective (a landing or an exit of the atmosphere to orbit).

Constant-altitude flight can be achieved only if the spacecraft lift force exactly counteracts the combined centrifugal and gravitational forces acting along the trajectory; that is,

$$\frac{1}{2}\rho V^2 \cos\phi\left[\frac{C_L A}{M}\right] = G\left(1 - \overline{V}^2\right) \qquad (1)$$

As the centrifugal and gravitational forces vary during entry, the lift force must be varied in a manner consistent with equation (1) so that a constant altitude flight path can be maintained. The roll-modulation technique requires that this lift be obtained by rolling the spacecraft until the desired component magnitude of the lift vector appears in

the local vertical plane. The roll-angle rate is considered instantaneous in all cases, and a finite roll rate changes entry performance slightly (ref. 14). Therefore, the vertical lift force will vary as needed between the full negative ($\phi = 180°$) and the full positive ($\phi = 0°$) spacecraft aerodynamic lift capability (the sign being determined by the instantaneous velocity of the vehicle). Subcircular velocities ($\overline{V} < 1$) require positive lift to maintain constant-altitude flight, whereas circular velocities ($\overline{V} = 1$) require no lift ($\phi = 90°$) and supercircular velocities ($\overline{V} > 1$) require negative lift (equation (1)).

A useful side effect gained from roll modulation is that of plane-change capability. Because the spacecraft lift vector is modulated between 0° and 180°, a component of the lift appears not only in the vertical plane but also in the lateral plane. Using this lateral maneuverability, the spacecraft can perform a plane change and thereby control either the coordinates of a landing site or the inclination of an orbit achieved after atmospheric exit. However, if a plane-change capability is not desired, it can be eliminated by alternating the lift-vector roll angle on both sides of the vertical, negating lateral components.

## Entry Corridor

Atmospheric capture of an entry vehicle is defined as having occurred when the vehicle kinetic energy has been dissipated by aerodynamic drag to such an extent that the vehicle no longer has the ability to exit the atmosphere without the application of an external force. The bounded set of entry trajectories that allow a vehicle to be captured by the atmosphere without violating vehicle loading constraints is termed the entry corridor.

Rather than defining an entry corridor as the difference between two bounding entry-flight-path angles, it is convenient to express it in terms of corridor depth and, hence, as the difference in vacuum periapsis radii of the two conic trajectories associated with the bounding entry angles. The upper bounding trajectory (overshoot boundary) is defined by the vacuum periapsis radius associated with the shallowest entry-flight-path angle at which the vehicle can be captured by the atmosphere using maximum negative lift capability ($\phi_E = 180°$). The lower bounding trajectory (undershoot boundary) is defined by the vacuum periapsis radius associated with the steepest entry-flight-path angle at which the vehicle can enter the atmosphere using maximum positive lift capability ($\phi_E = 0°$) without exceeding the system load limits. The maximum load considered acceptable on a manned vehicle is 10g. However, unmanned vehicles may have load capabilities in the range of several hundred g, a fact that often eliminates the undershoot boundary. For this reason, unmanned-vehicle trajectory-corridor depth is expressed only in terms of guidance capability reference corridors. Reference-corridor depths used in this study are 20 kilometers (10.8 n. mi.) and 50 kilometers (27 n. mi.) (ref. 15).

## Manned Missions

Manned missions to Venus involve the use of the atmosphere to decelerate the spacecraft from a high approach velocity to some velocity associated with a selected

parking orbit around Venus (ref. 16). Manned landing on the Venusian surface is not considered feasible because of the hostile surface conditions. Entry into the atmosphere is undertaken through a flight-path angle that approaches the overshoot boundary to ensure that an orbit can be attained after deceleration. Upon entering the atmosphere, the vehicle lift initially is directed downward ($\phi_E = 180^\circ$) so that the vehicle may be held in a region of significant atmospheric drag (figs. 2(a) and 2(c)). At a point designated as the inflection point ($\dot{\gamma} = 0$), the lift vector is modulated to an upright position ($\phi = 0^\circ$). When a flight-path angle of $0^\circ$ ($\gamma = 0^\circ$) is attained, the lift vector is modulated to that value of negative lift which imparts to the vehicle the trajectory characteristics of a constant-altitude flight path. The altitude at which $\gamma = 0^\circ$ is designated the pullout altitude $h_{pt}$. After pullout, the lift-vector roll angle is adjusted to maintain constant-altitude flight until the proper velocity-density conditions are achieved for initiation of the atmospheric exit maneuver. The exit maneuver is undertaken by reducing the vehicle roll angle until there is sufficient positive lift to force the vehicle out of the atmosphere with the desired state-vector characteristics.

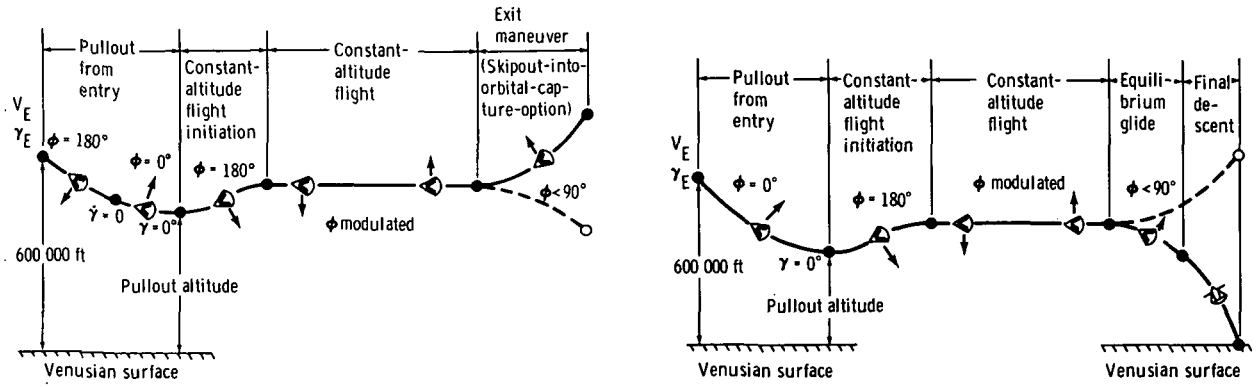


(a) Trajectory near the overshoot boundary.

(b) Trajectory near the undershoot boundary.

Figure 2.- Venus aerobraking maneuver.

## Unmanned Missions

Unmanned exploratory probes have a broader spectrum of entry capabilities than manned exploratory probes. These broader capabilities are reflected in and governed by the three primary probe-delivery techniques. The first technique, direct Earth launch, subjects the probe to severe loading conditions upon hypervelocity atmospheric entry at Venus. The second and third probe-delivery techniques, although yielding a reduced load level, are dependent on missions of a parent vehicle to near-Venus space. In each case, probes are released from the parent vehicle and are guided to either an orbit around Venus or a descent to the surface. Probes released by a parent vehicle that is in a Venus swingby trajectory enter the Venus atmosphere at velocities in excess of parabolic velocity. However, a lesser entry velocity is achieved by probes released from a parent vehicle that has attained an orbit around Venus.

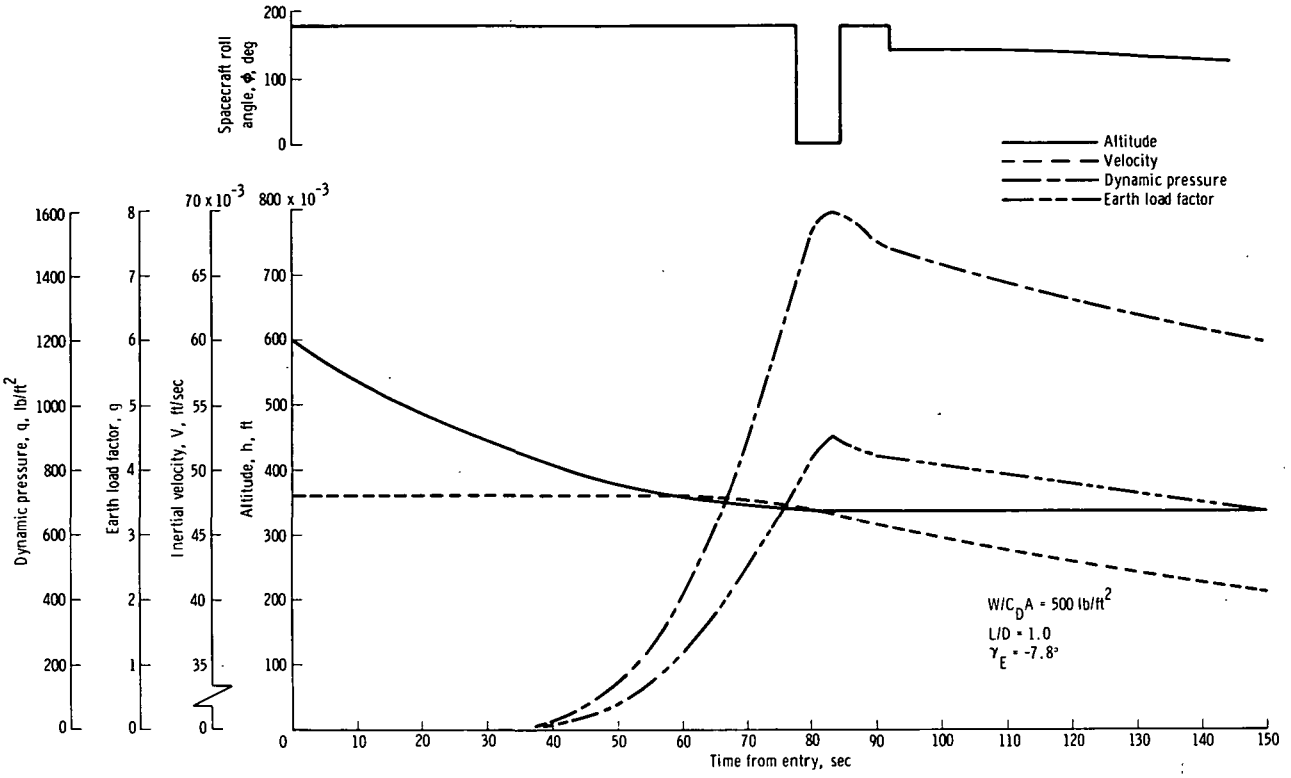


(c) Representative trajectory profile near the overshoot boundary.

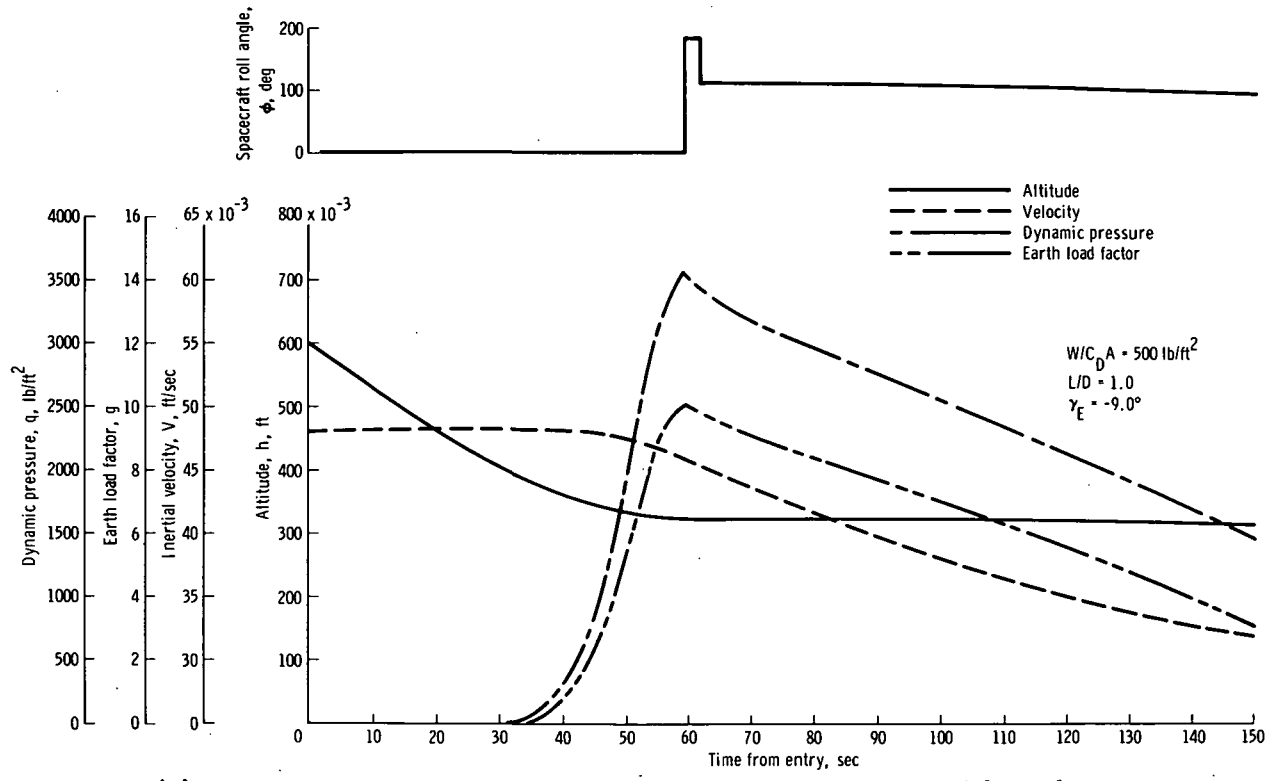


(d) Representative trajectory profile near the undershoot boundary.

Figure 2.- Concluded.

Probe entry capabilities associated with these delivery techniques range from a zero-lift ballistic entry to entry controlled by lift-vector roll modulation. Lifting probes may perform an aerobraking capture with a subsequent skipout into orbit, as discussed previously for manned missions, or they may land on the planet surface. Lifting-probe lander missions are similar to their orbiter counterparts in that they depend on the Venusian atmosphere for deceleration. Where it is desirable for aerobraker orbiter missions to enter the atmosphere at the overshoot boundary, lander-mission entry-flight-path angles approach the undershoot boundary, eliminating the danger of skipout. The lift vector initially is directed upward ($\phi_E = 0°$) to reduce the inertial load (figs. 2(b) and 2(d)). When the flight-path angle becomes zero ($\gamma = 0°$), the lift vector is rotated to that value that places the vehicle in a constant-altitude flight path. Then, constant-altitude flight is maintained until sufficient deceleration causes the vehicle lift and centrifugal forces to become ineffective in counteracting the gravitational force of the planet.

## Baseline Spacecraft and Trajectory Parameters

A representative range of manned and unmanned spacecraft characteristics was selected as indicative of planetary-spacecraft systems. Unmanned probes were assigned a ballistic parameter range of 0.5 to 2.0 slug/ft$^2$ and lift to drag (L/D) capabilities of 0 and 0.25. Manned entry vehicles were assigned a broad range of ballistic-parameter values to encompass the many feasible manned-mission modes. Manned entry vehicles, similar to Apollo-type spacecraft, that are released to entry from a larger manned vehicle have ballistic-parameter values of from 100 to 300 lb/ft$^2$. Ballistic parameters of intermediate sized manned vehicles range from approximately 300 to 600 lb/ft$^2$, whereas ballistic-parameter values for the larger manned aerobrakers range from 600 to 1000 lb/ft$^2$. Manned vehicle L/D capabilities were considered to be 0.25, 0.50, and 1.00.

Atmospheric entry velocities examined for manned-mission operations at Venus were 36 000 and 48 000 ft/sec, which are representative parabolic and hyperbolic approach velocities. Unmanned probes undergoing atmospheric entry at parabolic and hyperbolic velocities also were considered to perform entry operations from an orbit at velocities of 24 000 and 30 000 ft/sec.

# RESULTS AND DISCUSSION

## Manned Entry

The vacuum periapsis radii of the undershoot and overshoot boundaries are shown in figure 3 as a function of the spacecraft ballistic parameter for the manned L/D capabilities of 0.25, 0.50, and 1.00. The data for entry velocities of 36 000 and 48 000 ft/sec also are given in figure 3. In each case, the spacecraft ballistic parameter affects the undershoot and overshoot periapsis radii in a similar manner: an increase in the ballistic parameter slightly decreases the associated periapsis radius. Entry-corridor depth (as determined by the 10-g load-limit undershoot) is shown in figure 4 as a

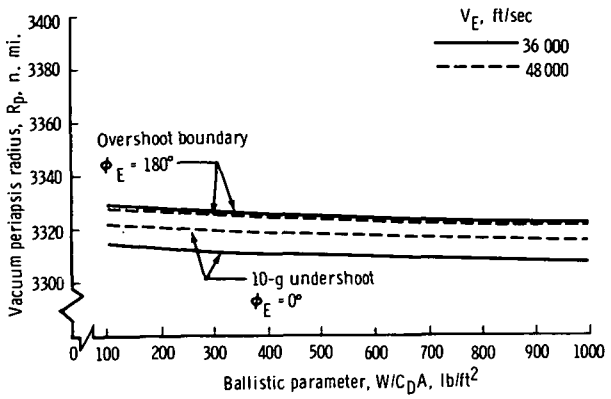


(a) L/D = 0.25.

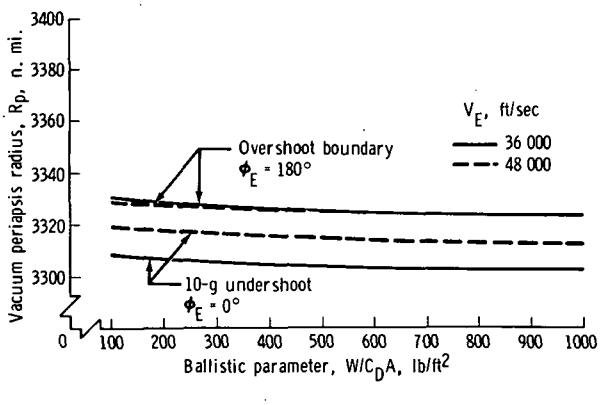


(b) L/D = 0.50.

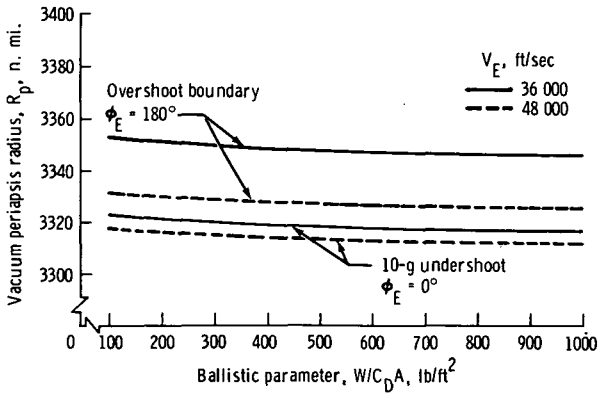


(c) L/D = 1.00.

Figure 3.- Undershoot and overshoot boundary vacuum periapsis radii as a function of spacecraft ballistic parameter.

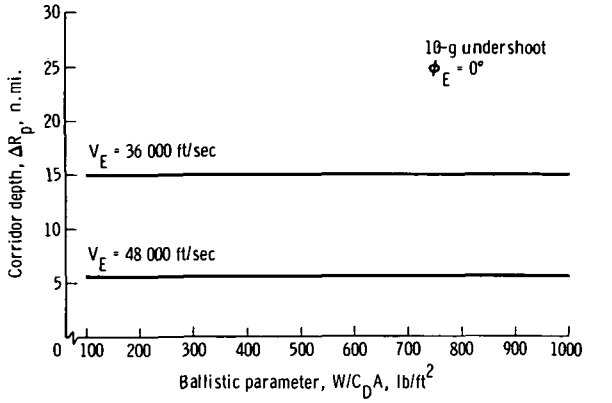


(a) L/D = 0.25.

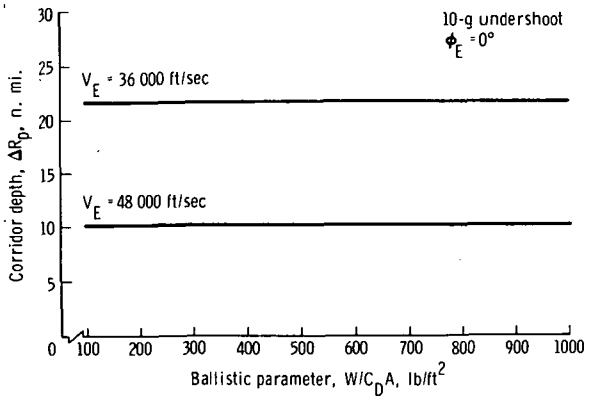


(b) L/D = 0.50.

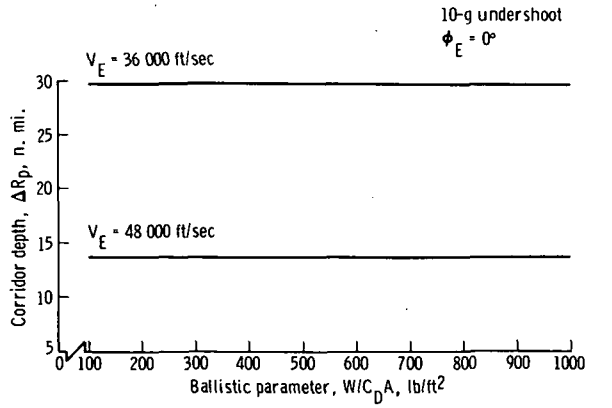


(c) L/D = 1.00.

Figure 4.- Entry-corridor depth as a function of spacecraft ballistic parameter.

function of the spacecraft ballistic parameter. Entry velocities of 36 000 and 48 000 ft/sec were considered, as were L/D values of 0.25, 0.50, and 1.00. From these values, the entry-corridor depth was found to be insensitive to variations in a ballistic parameter having values between 100 and 1000 lb/ft$^2$. However, the spacecraft ballistic parameter does influence the location of the corridor in the atmosphere; the lower the ballistic parameter the higher the corridor. The undershoot and overshoot boundary entry flight-path angles are presented as a function of the spacecraft ballistic parameter in figure 5 for entry velocities of 36 000 and 48 000 ft/sec with L/D values of 0.25, 0.50, and 1.00. The entry angles were determined to the nearest 0.1°.

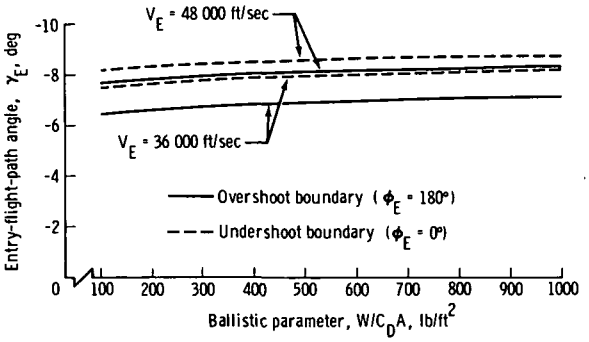


(a) L/D = 0.25.

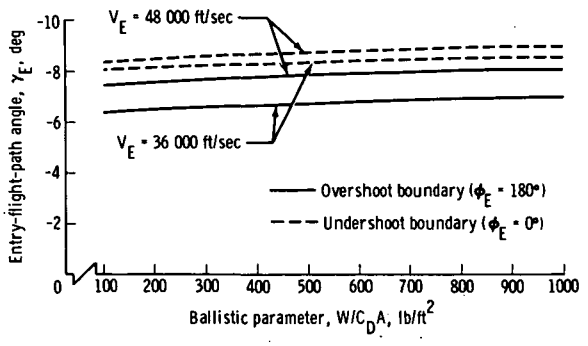


(b) L/D = 0.50.

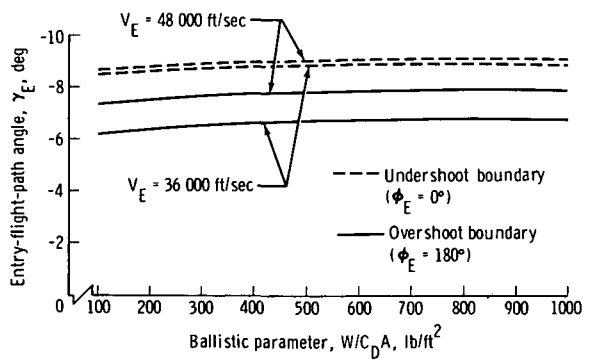


(c) L/D = 1.00.

Figure 5.- Undershoot and overshoot boundary entry-flight-path angles as a function of spacecraft ballistic parameter.

The maximum dynamic pressure as a function of the spacecraft ballistic parameter for the 10-g load-limit undershoot entry-flight-path angle is shown in figure 6. Each of the manned L/D capabilities had an increase in the maximum dynamic pressure with an increase in the spacecraft ballistic parameter for the entry velocities of 36 000 and 48 000 ft/sec.

The pullout altitude and velocity as a function of spacecraft ballistic parameter are presented in figure 7 for the undershoot boundary entry-flight-path angle. Entry velocities of 36 000 and 48 000 ft/sec were considered and vehicle L/D capabilities of 0.25, 0.50, and 1.00 executed through a 0° initial roll angle. Although the pullout altitude was lowered by an increase in the spacecraft ballistic parameter, the pullout velocity was not affected by ballistic-parameter variance. The pullout altitudes and velocities associated with the overshoot boundary entry-flight-path angles ($\phi_E$ = 180°) show much the same trends (fig. 8) as those for the undershoot entry-flight-path angles.

However, the overshoot pullout altitudes are somewhat higher than those for the undershoot. The velocities associated with both the overshoot and undershoot and pullout maneuvers are essentially the same.

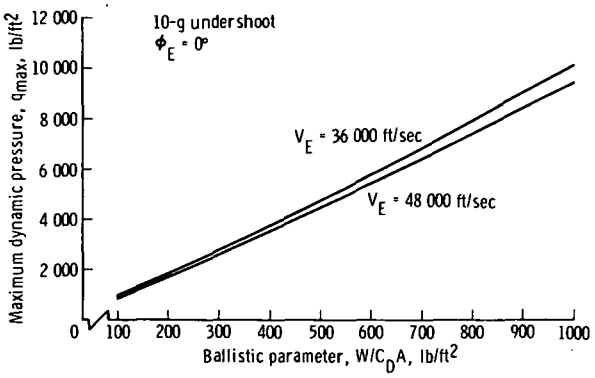


(a) L/D = 0.25.

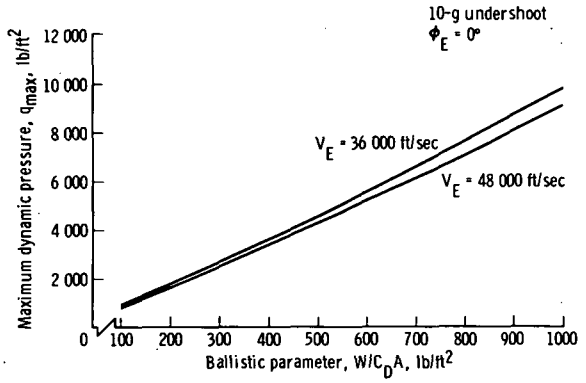


(b) L/D = 0.50.

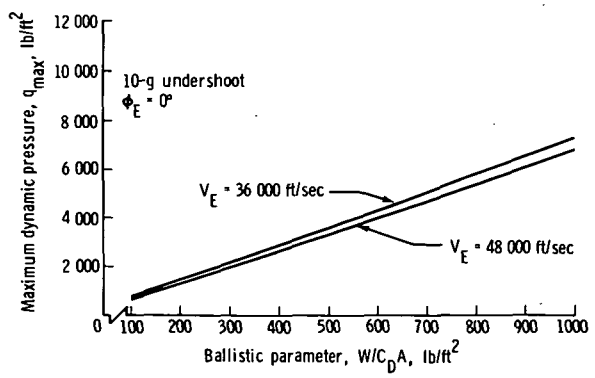


(c) L/D = 1.00.

Figure 6.- Undershoot boundary maximum dynamic pressure as a function of spacecraft ballistic parameter.

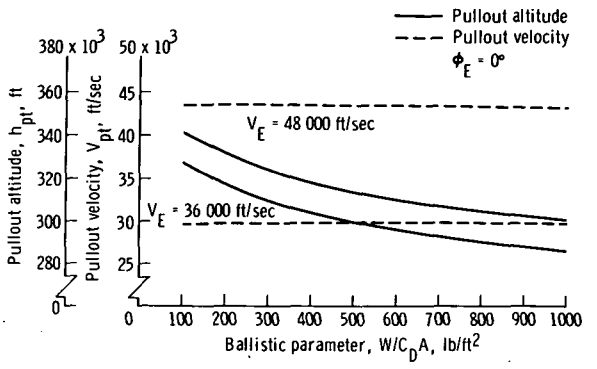


(a) L/D = 0.25.

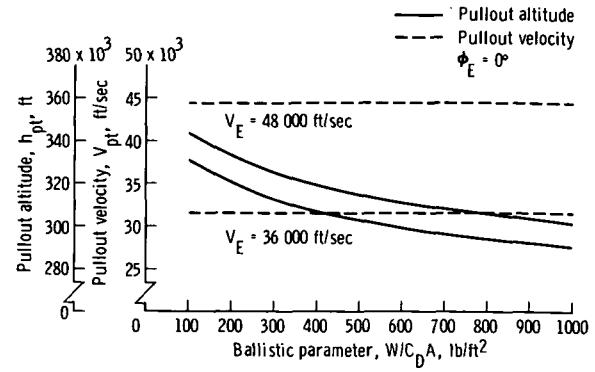


(b) L/D = 0.50.

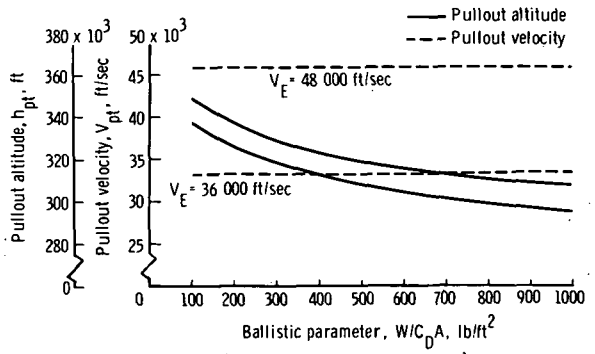


(c) L/D = 1.00.

Figure 7.- Undershoot boundary pullout altitude and velocity as a function of spacecraft ballistic parameter.

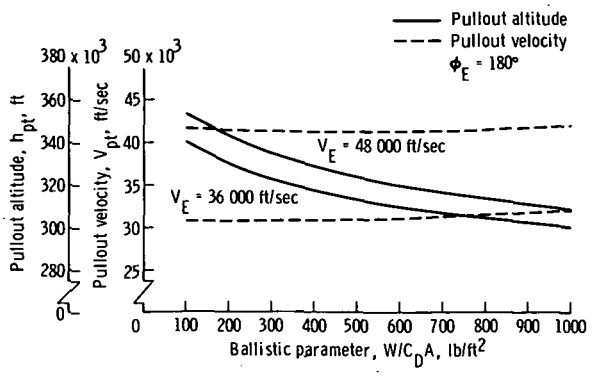


(a) L/D = 0.25.

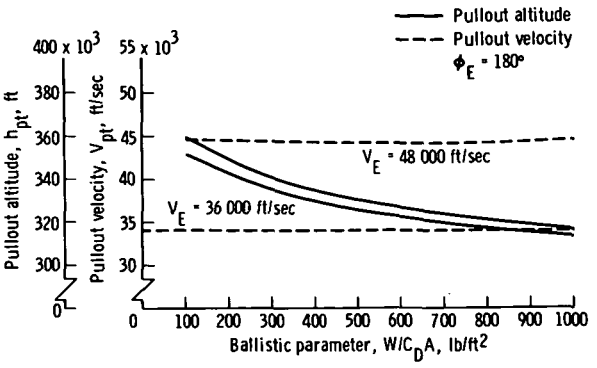


(b) L/D = 0.50.

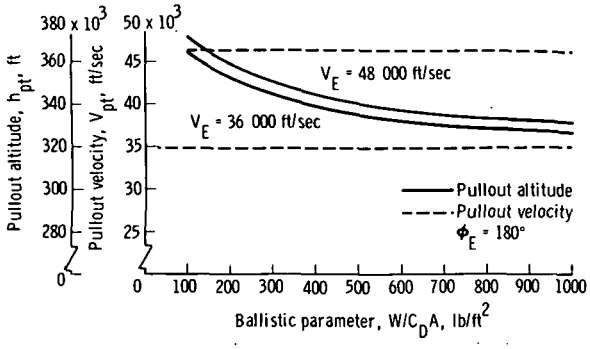


(c) L/D = 1.00.

Figure 8.- Overshoot boundary pullout altitude and velocity as a function of spacecraft ballistic parameter.

In the presentation of parameters as a function of entry velocity, values of 36 000 and 48 000 ft/sec were examined, and a straight-line interpolation was used for the parameter values at intermediate points. Deviations from the straight-line approximation are small in this velocity range.

The vacuum periapsis radii of both the undershoot and overshoot trajectories are presented as functions of the entry velocity in figures 9(a) to 9(c). A spacecraft ballistic parameter of 100 lb/ft$^2$ and L/D capabilities of 0.25, 0.50, and 1.00 were considered. Similarly, the vacuum periapsis radii of the undershoot and overshoot trajectories are plotted as a function of entry velocity (figs. 9(d) to 9(i)) for spacecraft ballistic parameters of 500 and 1000 lb/ft$^2$. In each case, an increase in entry velocity raises the periapsis radius of the undershoot trajectory and lowers the periapsis radius of the corresponding overshoot trajectory. Corridor depth as a function of entry velocity for spacecraft L/D values of 0.25, 0.50, and 1.00 is presented in figure 10. Remembering that corridor depth is insensitive to changes of the ballistic parameter, an increase in entry velocity reduces the corridor depth for all considered ballistic-parameter values. The overshoot entry-flight-path angle is presented as a function of the entry velocity (fig. 11) for spacecraft L/D capabilities of 0.25, 0.50, and 1.00. Expectedly, an increasing entry velocity necessitates an increase in the entry flight-path angle for a successful atmospheric capture.

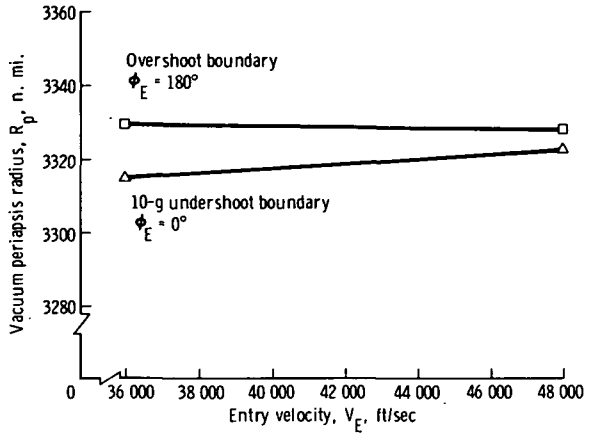


(a) L/D = 0.25, $W/C_DA$ = 100 lb/ft$^2$.

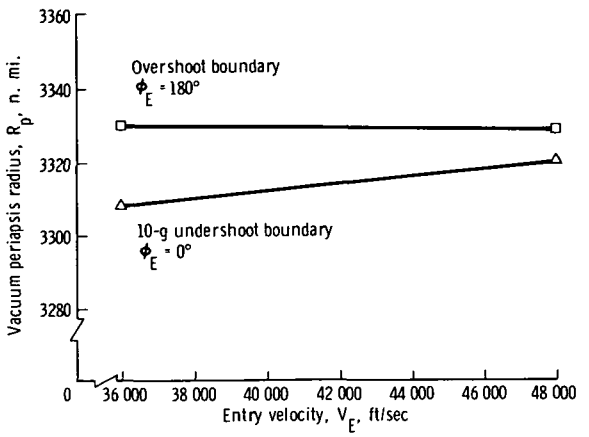


(b) L/D = 0.50, $W/C_DA$ = 100 lb/ft$^2$.

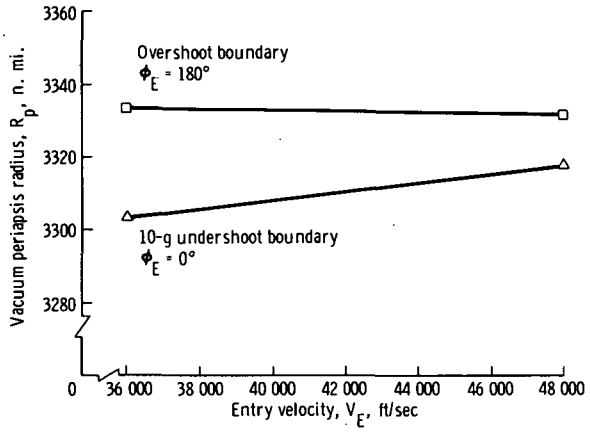


(c) L/D = 1.00, $W/C_DA$ = 100 lb/ft$^2$.

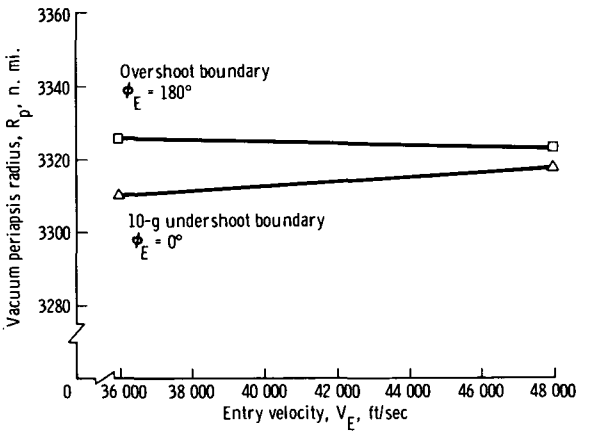


(d) L/D = 0.25, $W/C_DA$ = 500 lb/ft$^2$.

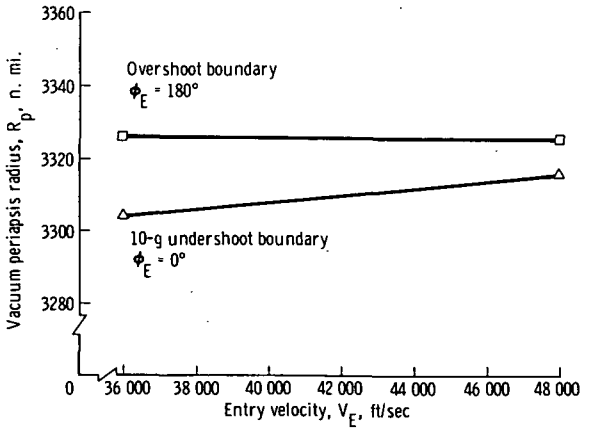


(e) L/D = 0.50, $W/C_DA$ = 500 lb/ft$^2$.

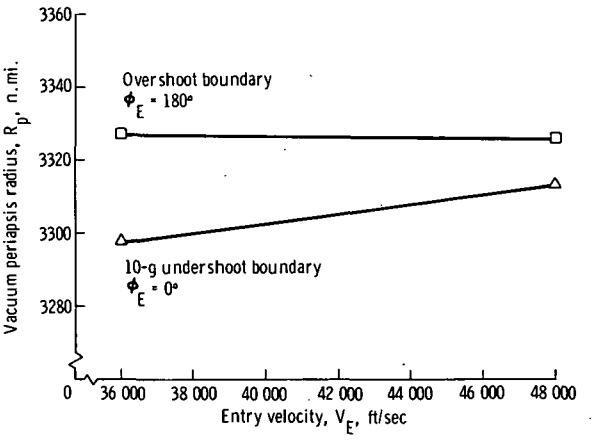


(f) L/D = 1.00, $W/C_DA$ = 500 lb/ft$^2$.

Figure 9.- Undershoot and overshoot boundary vacuum periapsis radii as a function of entry velocity.

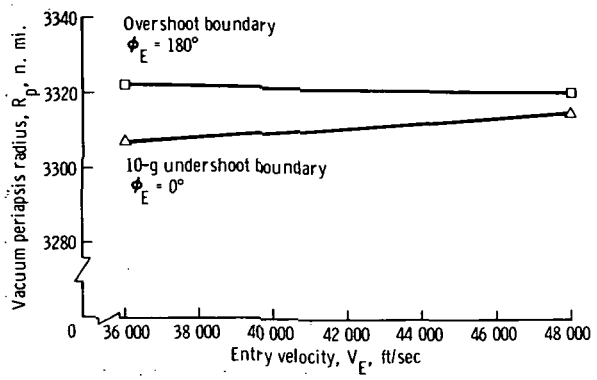


(g) L/D = 0.25, $W/C_DA$ = 1000 lb/ft$^2$.

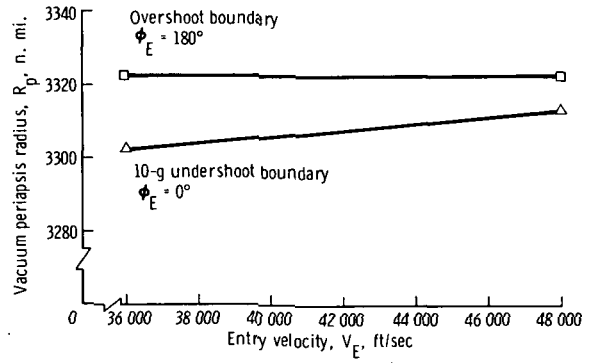


(h) L/D = 0.50, $W/C_DA$ = 1000 lb/ft$^2$.

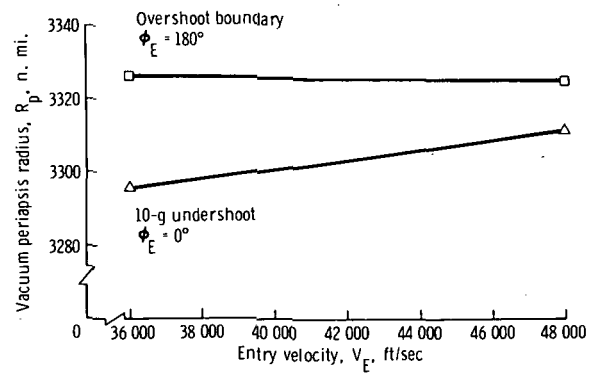


(i) L/D = 1.00, $W/C_DA$ = 1000 lb/ft$^2$.

Figure 9.- Concluded.

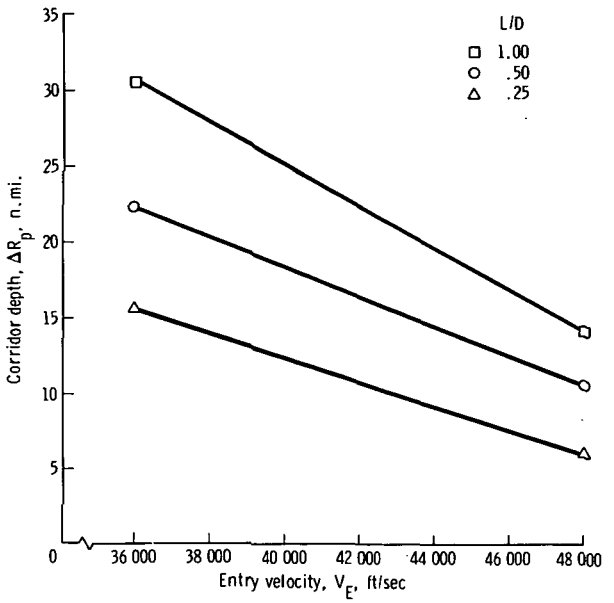


Figure 10.- Entry-corridor depth as a function of entry velocity.

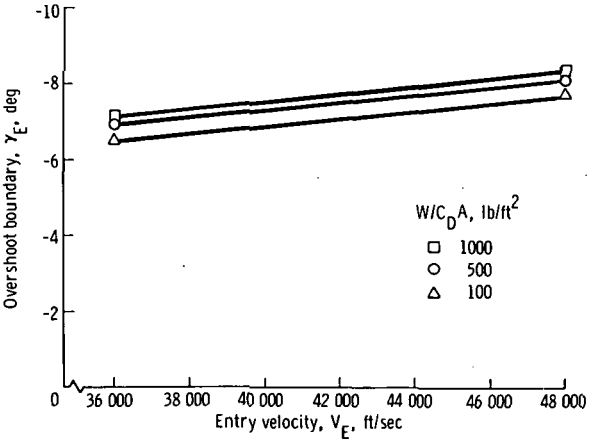


(a) L/D = 0.25.

Figure 11.- Overshoot boundary entry-flight-path angle as a function of entry velocity.

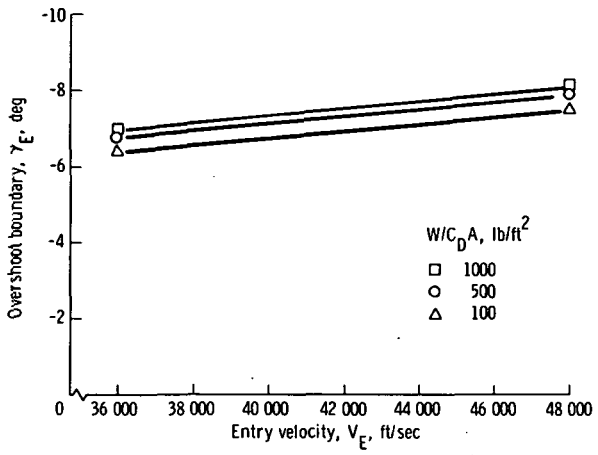


(b) L/D = 0.50.

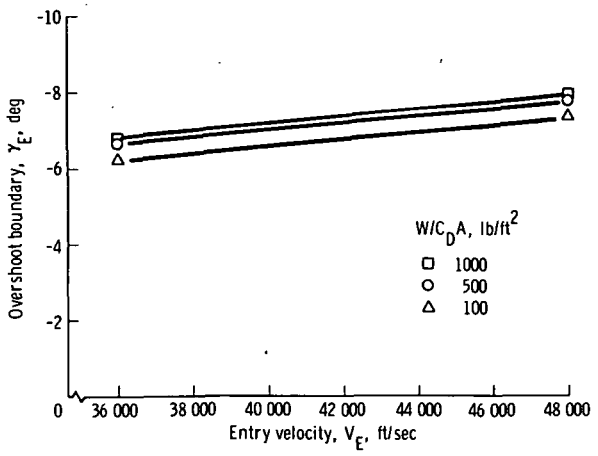


(c) L/D = 1.00.

Figure 11. - Concluded.

Maximum dynamic pressure as a function of entry velocity at the 10-g undershoot boundary entry-flight-path angle for L/D values of 0.25, 0.50, and 1.00 is shown in figure 12. For higher values of the spacecraft ballistic parameter, an increase in entry velocity decreases the maximum dynamic pressure slightly. This is because, as the entry velocity increases, the 10-g undershoot entry angle undergoes a subsequent decrease. Entry-velocity variance between 36 000 and 48 000 ft/sec has little or no effect on the maximum dynamic pressure for low ballistic-parameter values.

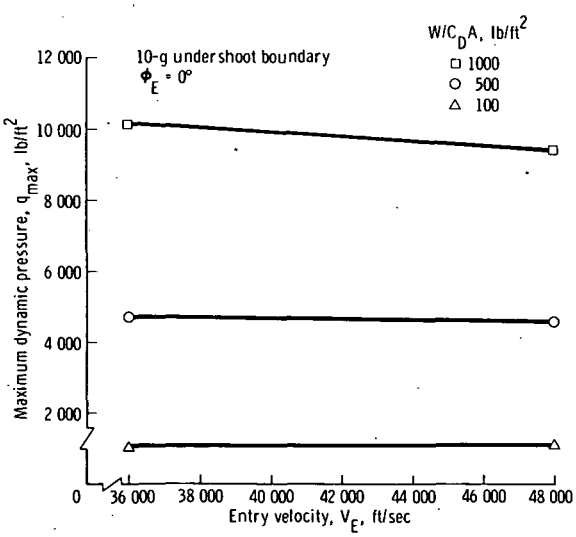


(a) L/D = 0.25.

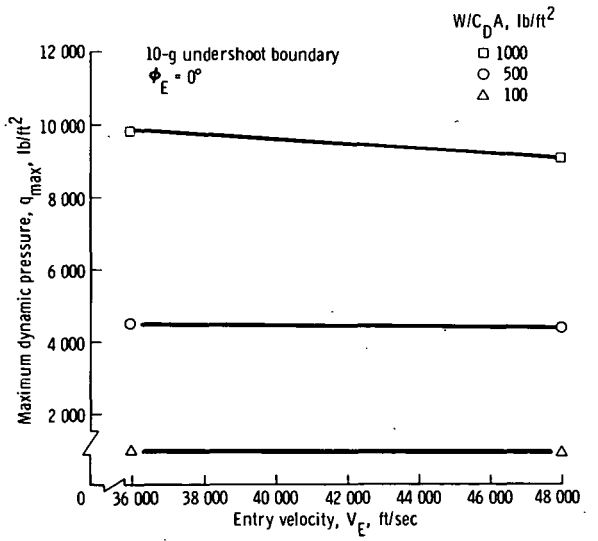


(b) L/D = 0.50.

Figure 12. - Undershoot boundary maximum dynamic pressure as a function of entry velocity.

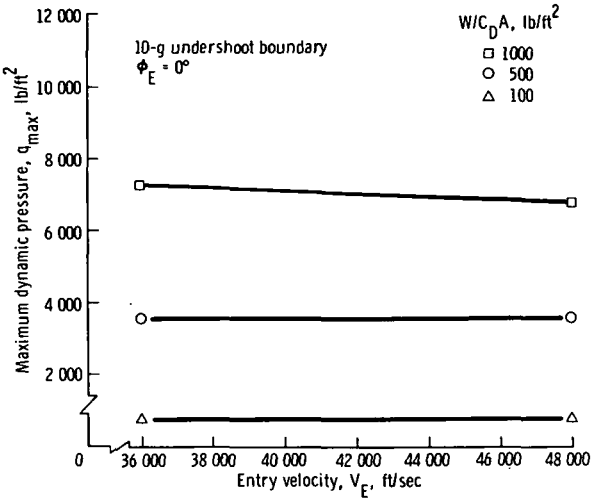


(c) L/D = 1.00.

Figure 12.- Concluded.

Pullout altitude as a function of entry velocity is presented (fig. 13) for the undershoot boundary entry-flight-path angle ($\phi_E = 0°$). Under these conditions, the pullout altitude increases with an increase in entry velocity. Similarly, the pullout altitude as a function of entry velocity at the overshoot boundary is presented in figure 14. However, in this instance the pullout altitude decreases with increasing velocity.

Corridor depth as a function of vehicle L/D capability is presented in figure 15 for entry velocities of 36 000 and 48 000 ft/sec. Each entry velocity undergoes a definite increase in corridor depth with an increase in the lift-to-drag ratio. The overshoot boundary entry-flight-path angle as a function of the spacecraft L/D capability is presented (fig. 16) for ballistic parameter values of 100 lb/ft$^2$, 500 lb/ft$^2$, and 1000 lb/ft$^2$ at entry velocities of 36 000 and 48 000 ft/sec. Given a value of the spacecraft ballistic parameter, the overshoot boundary entry angle decreases very slightly with increasing L/D values. The maximum dynamic pressure as a function of spacecraft L/D capability at the 10-g undershoot boundary entry-flight-path angle is

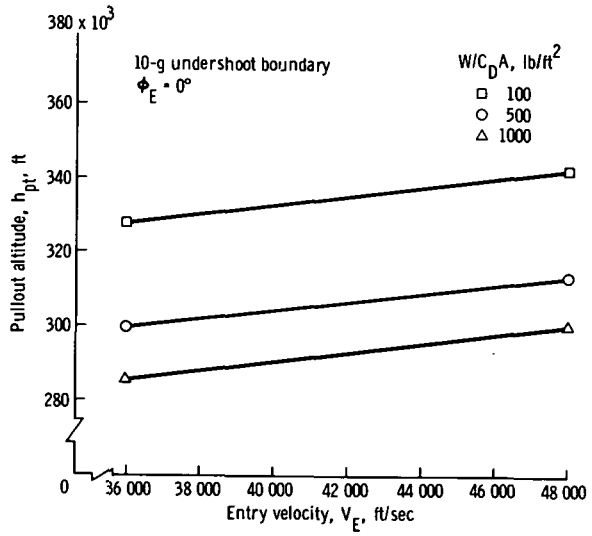


(a) L/D = 0.25.

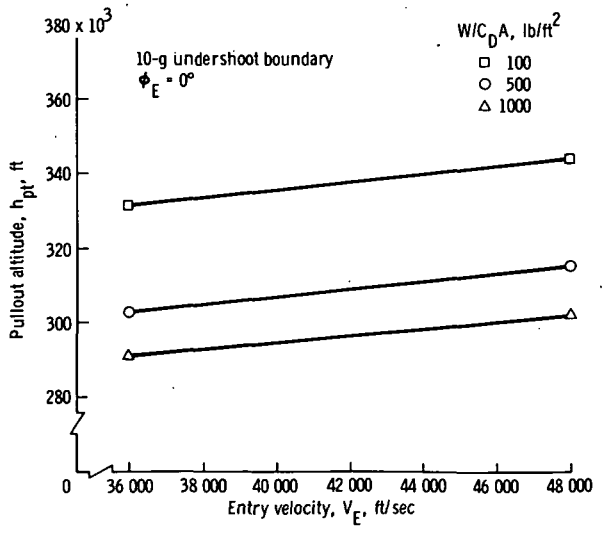


(b) L/D = 0.50.

Figure 13.- Undershoot boundary pullout altitude as a function of entry velocity.

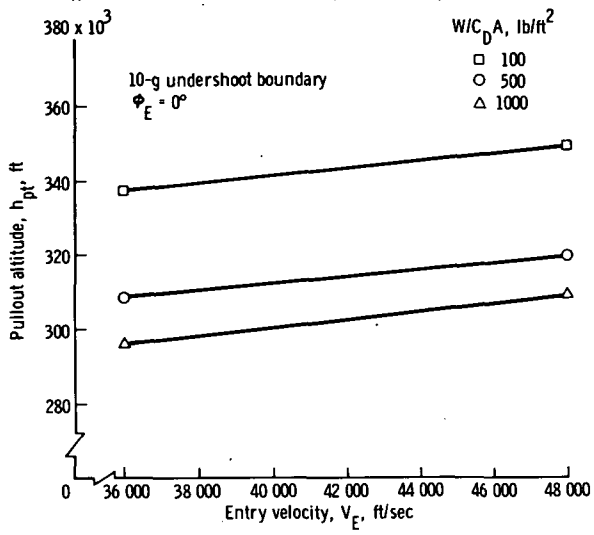


(c) L/D = 1.00.

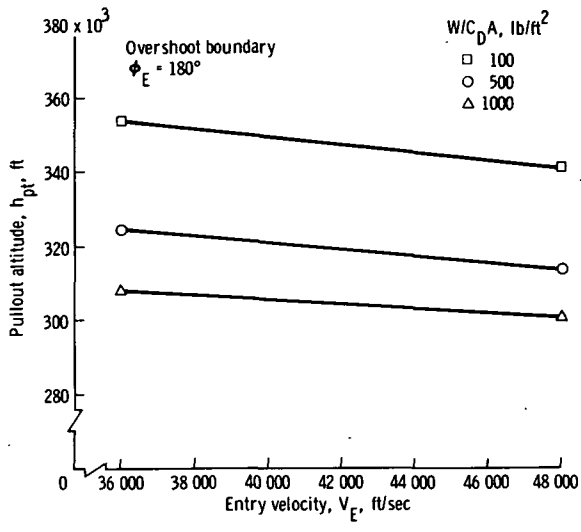


(a) L/D = 0.25.

Figure 13. - Concluded.

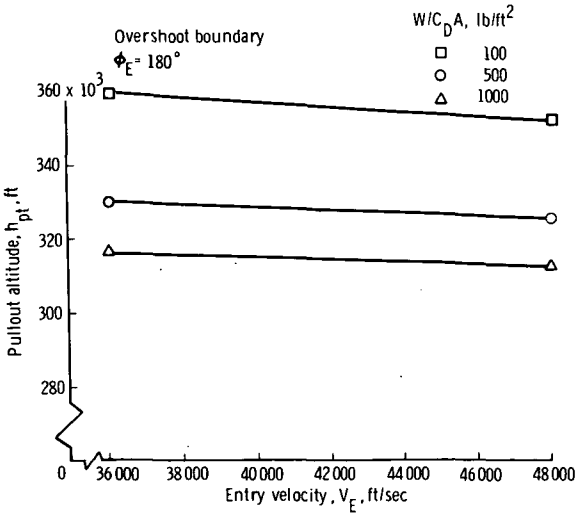


(b) L/D = 0.50.

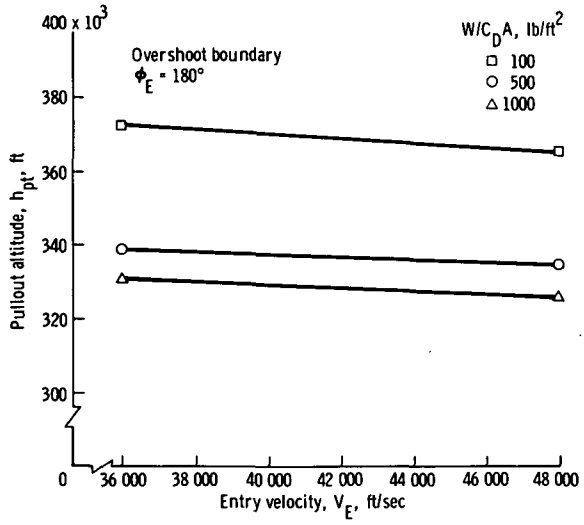


(c) L/D = 1.00.

Figure 14. - Overshoot boundary pullout altitude as a function of entry velocity.

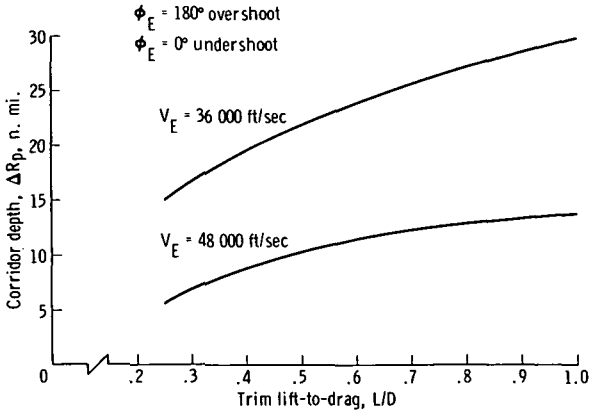


Figure 15.- Entry-corridor depth as a function of spacecraft trim lift-to-drag ratio.

given in figure 17. The maximum dynamic pressure encountered by vehicles that have a large ballistic parameter decreases noticeably with an increase in values of the lift-to-drag ratio. However, vehicles that have a smaller ballistic parameter undergo only a slight decrease in maximum dynamic pressure with increasing L/D. The pullout altitude as a function of spacecraft L/D capability at the undershoot boundary is presented in figure 18. Similarly, the pullout altitude as a function of L/D for entries at the overshoot boundary is presented in figure 19. In both cases, increasing L/D values raise the pullout altitude for a given spacecraft ballistic-parameter value.

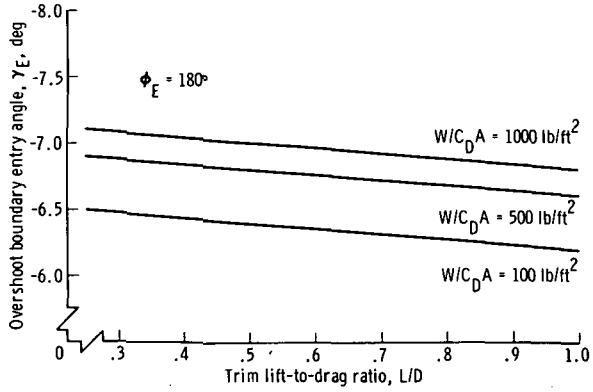


(a) $V_E$ = 36 000 ft/sec.

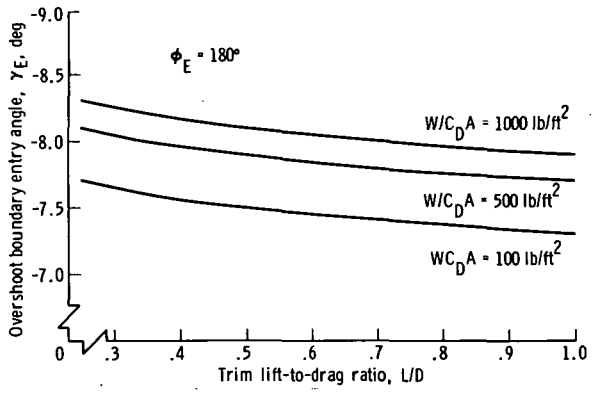


(b) $V_E$ = 48 000 ft/sec.

Figure 16.- Overshoot boundary entry flight path angle as a function of spacecraft trim lift-to-drag ratio.

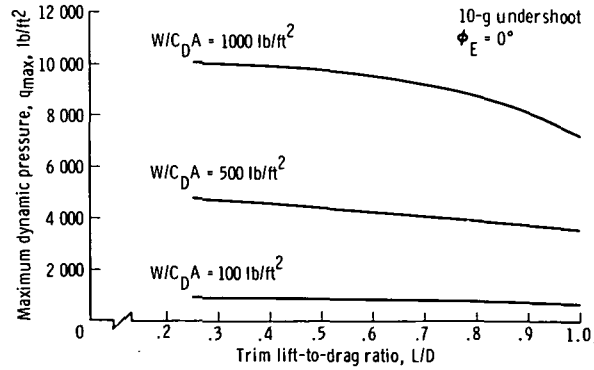


(a) $V_E$ = 36 000 ft/sec.

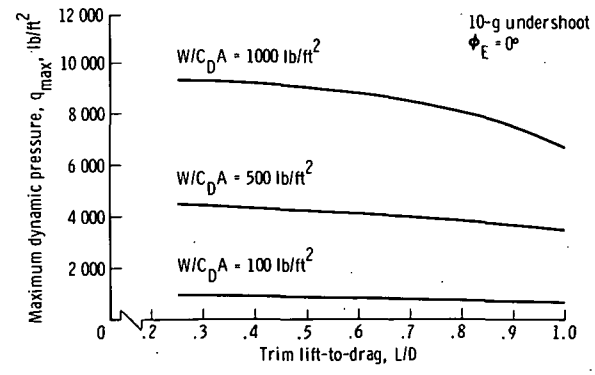


(b) $V_E$ = 48 000 ft/sec.

Figure 17.- Undershoot boundary maximum dynamic pressure as a function of spacecraft trim lift-to-drag ratio.

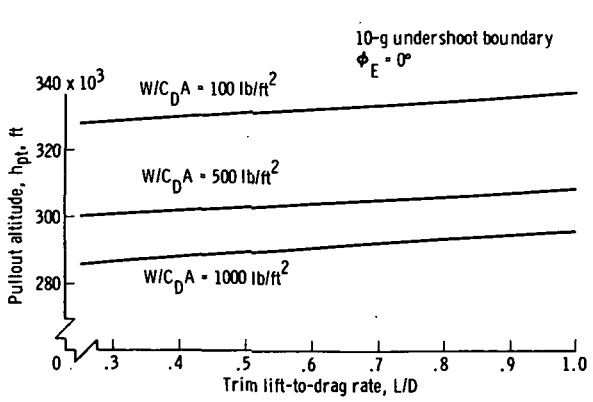


(a) $V_E$ = 36 000 ft/sec.

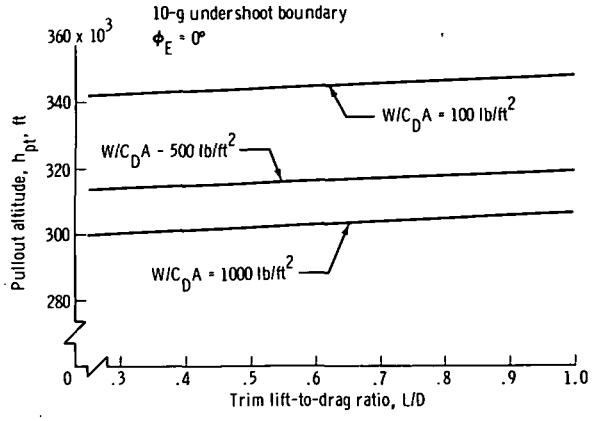


(b) $V_E$ = 48 000 ft/sec.

Figure 18. - Undershoot boundary pullout altitude as a function of spacecraft trim lift-to-drag ratio.

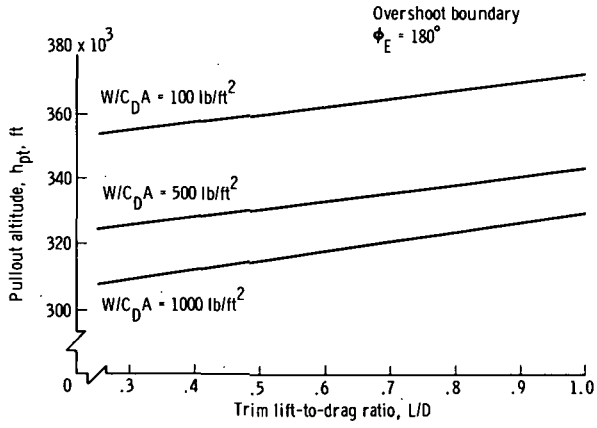


(a) $V_E$ = 36 000 ft/sec.

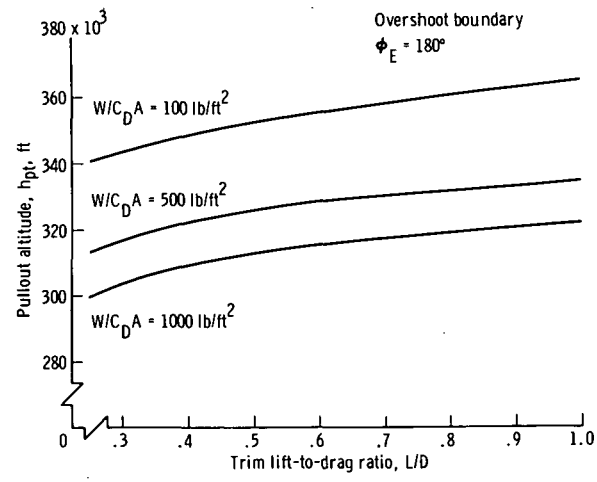


(b) $V_E$ = 48 000 ft/sec.

Figure 19. - Overshoot boundary pullout altitude as a function of spacecraft trim lift-to-drag ratio.

Corridor depth as a function of entry velocity for an atmospheric density dispersion of ±50 percent of the Venusian density profile data points is presented in figure 20. The corridor reduction was calculated by taking into account the effects of both the decrease in the undershoot entry angle caused by a positive 50-percent density dispersion and the increase in the overshoot entry angle caused by a negative 50-percent density dispersion. A spacecraft with an L/D capability of 0.50 (fig. 20(a)) undergoes a corridor-depth reduction of approximately 3.5 n. mi. with a ±50 percent density

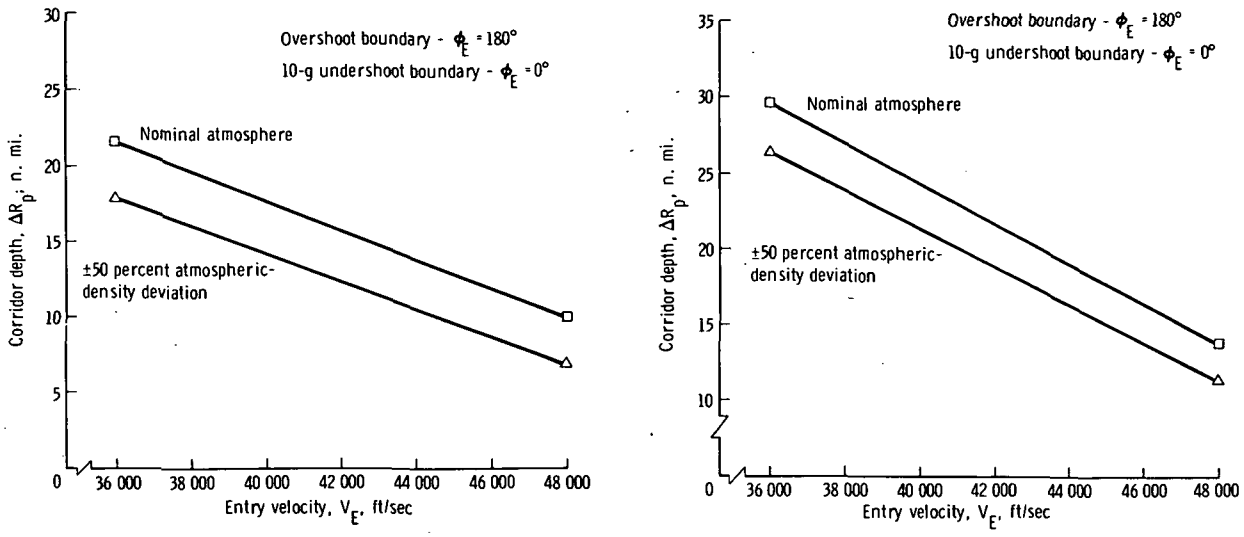


(a) L/D = 0.50.

(b) L/D = 1.00.

Figure 20.- Entry-corridor depth as a function of entry velocity for ±50 percent atmospheric-density deviation.

deviation over the range of considered velocities. This same deviation reduces the corridor depth by approximately 3.0 n. mi. for a spacecraft having an L/D capability of 1.00 (fig. 20(b)).

## Unmanned-Probe Entry

Data obtained from the analysis of probe atmospheric entry are divided into two sections. The first section involves entry at approach velocities of 36 000 and 48 000 ft/sec. The second section involves entry from orbit at representative velocities of 24 000 and 30 000 ft/sec.

The overshoot boundary entry-flight-path angle as a function of vehicle ballistic parameter for entry velocities of 36 000 and 48 000 ft/sec is presented in figure 21. For each of the considered L/D values of 0 and 0.25, an increasing ballistic parameter tended to increase slightly the overshoot entry angle. The corresponding vacuum periapsis radii are shown in figure 22. The entry-flight-path angle as a function of spacecraft ballistic parameter is depicted in figure 23 with reference to the overshoot boundary, the 20-kilometer (10.8-n. mi.) entry corridor, and the 50-kilometer (27-n. mi.) entry corridor. An increasing ballistic parameter prompts a very slight increase in the entry angle in each case at an entry velocity of 36 000 ft/sec (figs. 23(a) and 23(b)). Entry-flight-path angles for an entry velocity of 48 000 ft/sec (figs. 23(c) and 23(d)) have a similar reaction to an increase of ballistic parameter.

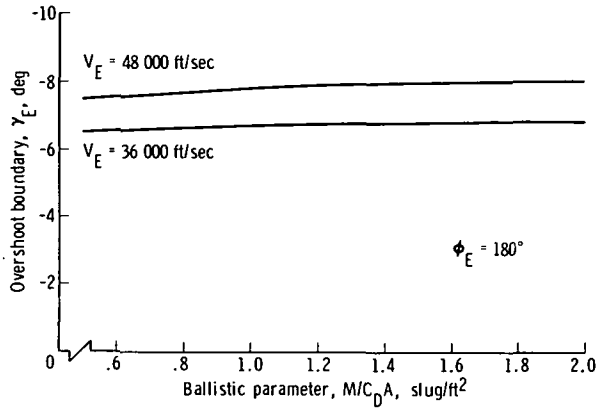


(a) L/D = 0.

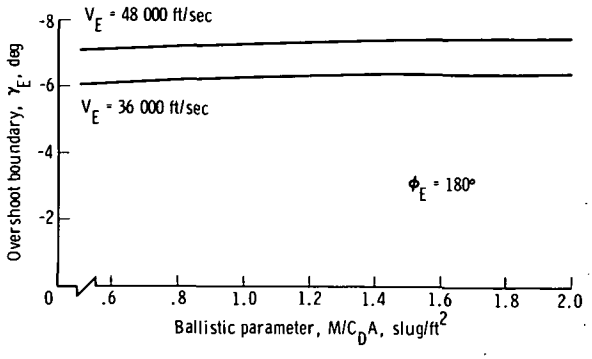


(b) L/D = 0.25.

Figure 21. - Overshoot boundary entry-flight-path angle as a function of spacecraft ballistic parameter.

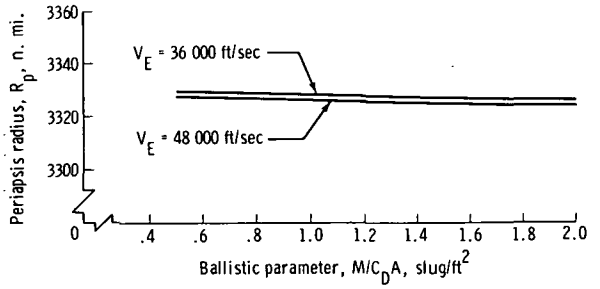


(a) L/D = 0.

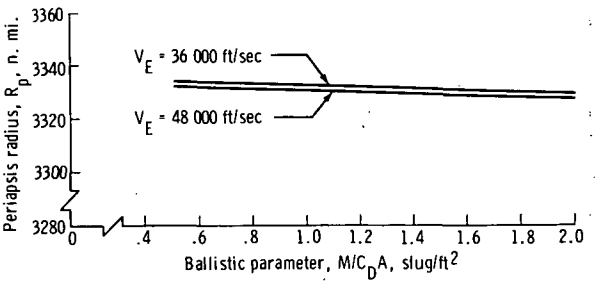


(b) L/D = 0.25.

Figure 22. - Overshoot boundary vacuum periapsis radius as a function of spacecraft ballistic parameter.

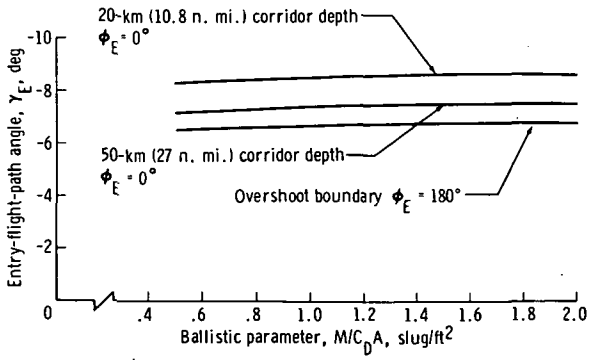


(a) L/D = 0, $V_E$ = 36 000 ft/sec.

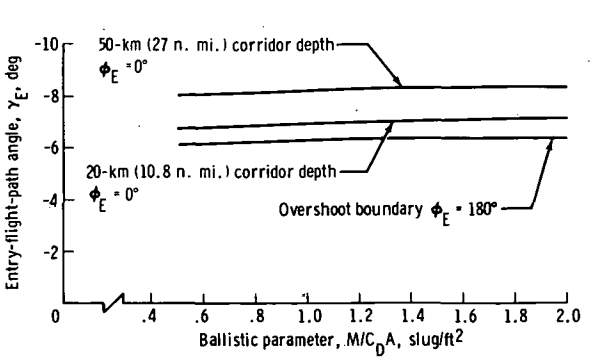


(b) L/D = 0.25, $V_E$ = 36 000 ft/sec.

Figure 23. - Entry-flight-path angle as a function of spacecraft ballistic parameter for the overshoot boundary, the 10.8-n. mi. entry corridor, and the 27-n. mi. entry corridor.

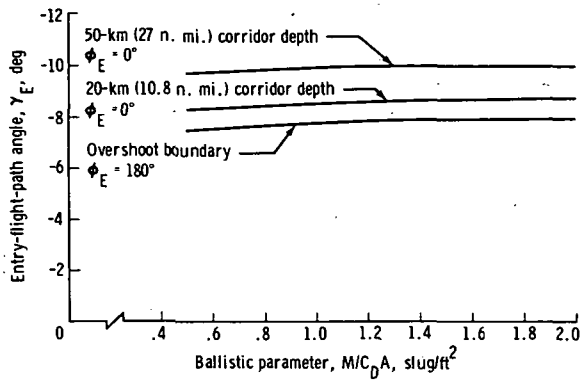


(c) L/D = 0, $V_E$ = 48 000 ft/sec.

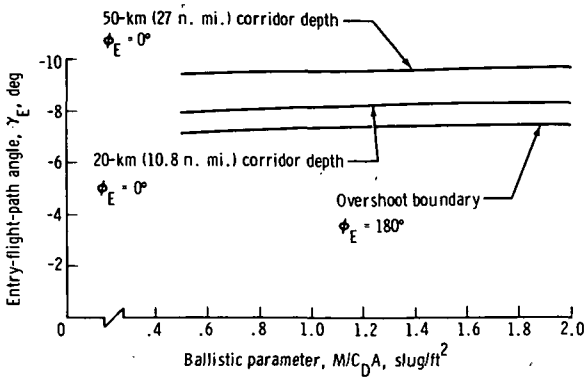


(d) L/D = 0.25, $V_E$ = 48 000 ft/sec.

Figure 23. - Concluded.

The maximum Earth load factor for entry operations at the overshoot boundary ($\phi_E = 180°$), the 10.8-n. mi. entry corridor ($\phi_E = 0°$), the 27-n. mi. entry corridor ($\phi_E = 0°$), and direct entry ($\gamma_E = -90°$) show no appreciable variance with increasing ballistic parameter (fig. 24). An examination of the maximum dynamic pressure incurred under these same entry conditions reveals that an increasing spacecraft ballistic parameter increases the respective maximum dynamic pressure (fig. 25).

The variance of overshoot boundary entry angle with entry velocity demonstrates a slightly augmented entry angle with increasing entry velocity (fig. 26). The entry-flight-path angle is shown in figure 27 as a function of the entry velocity for ballistic parameter values of 0.5, 1.0, 1.5, and 2.0 slug/ft$^2$ at the overshoot boundary, the 10.8-n. mi. entry corridor, and the 27-n. mi. entry corridor. Each of the entry angles associated with these trajectories was increased by a corresponding increase in the entry velocity. The maximum Earth load factor as a function of the entry velocity

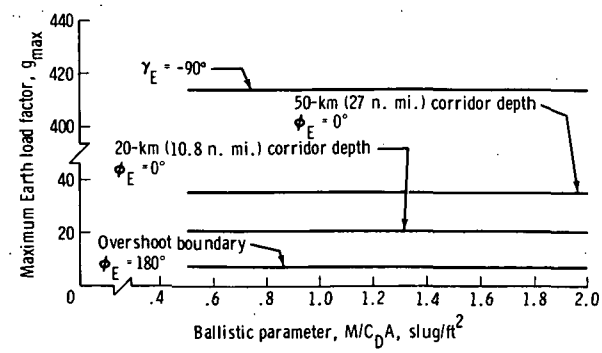


(a) L/D = 0, $V_E$ = 36 000 ft/sec.

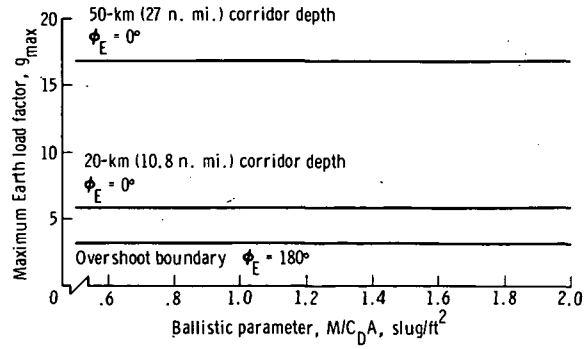


(b) L/D = 0.25, $V_E$ = 36 000 ft/sec.

Figure 24. - Maximum Earth load factor as a function of spacecraft ballistic parameter for the overshoot boundary, the 10.8-n. mi. entry corridor, the 27-n. mi. entry corridor, and direct entry.

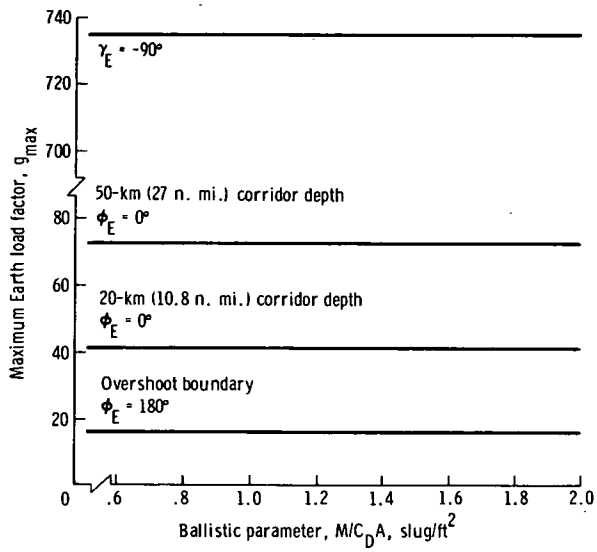


(c) L/D = 0, $V_E$ = 48 000 ft/sec.

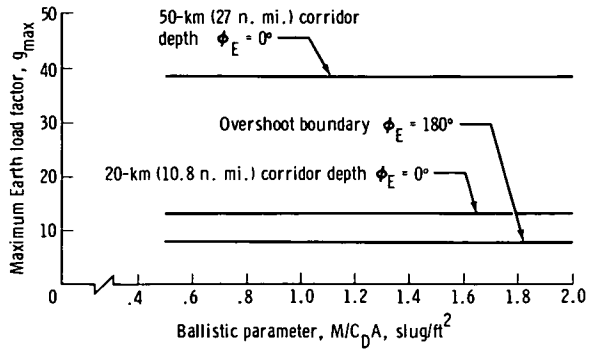


(d) L/D = 0.25, $V_E$ = 48 000 ft/sec.

Figure 24.- Concluded.

is presented in figure 28 for this same range of ballistic-parameter values. Considering this function for the overshoot boundary, the 10.8-n. mi. entry corridor, and the 27-n. mi. entry corridor reveals that an increase in entry velocity increases the maximum Earth load factor encountered at each trajectory. The corresponding data for the maximum dynamic pressure during entry are given in figure 29.

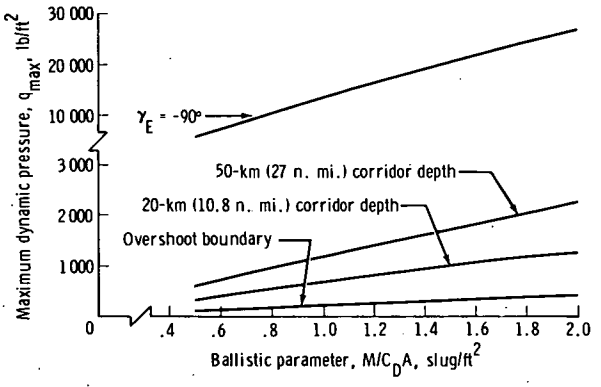


(a) L/D = 0, $V_E$ = 36 000 ft/sec.

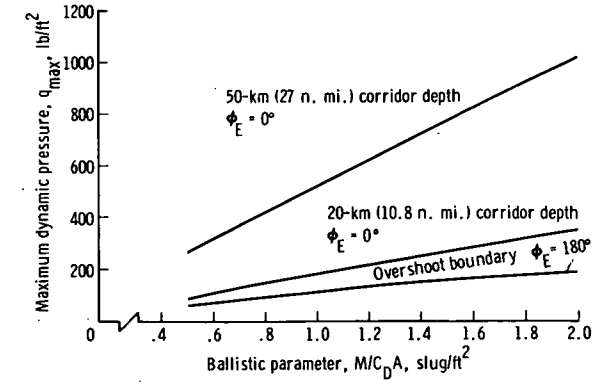


(b) L/D = 0.25, $V_E$ 36 000 ft/sec.

Figure 25.- Maximum dynamic pressure as a function of spacecraft ballistic parameter for the overshoot boundary, the 10.8-n. mi. entry corridor, the 27-n. mi. entry corridor, and direct entry.

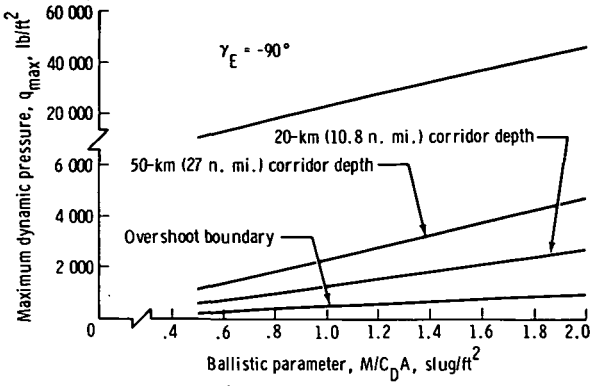


(c) L/D = 0, $V_E$ = 48 000 ft/sec.

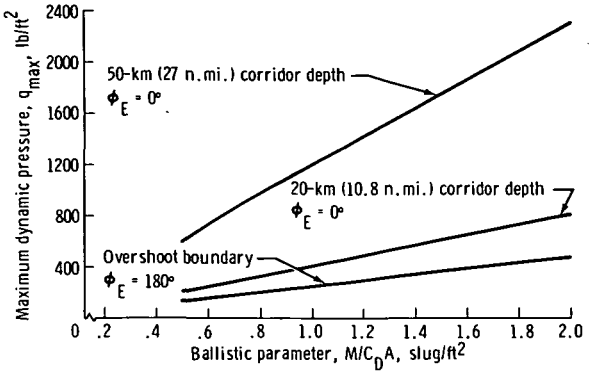


(d) L/D = 0.25, $V_E$ = 48 000 ft/sec.

Figure 25.- Concluded.

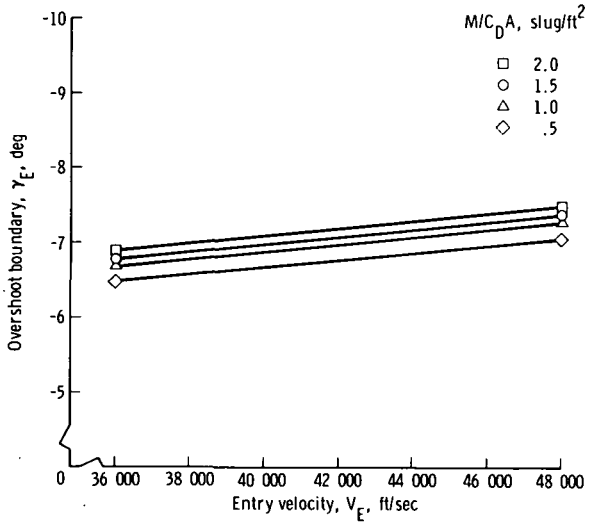


(a) L/D = 0.

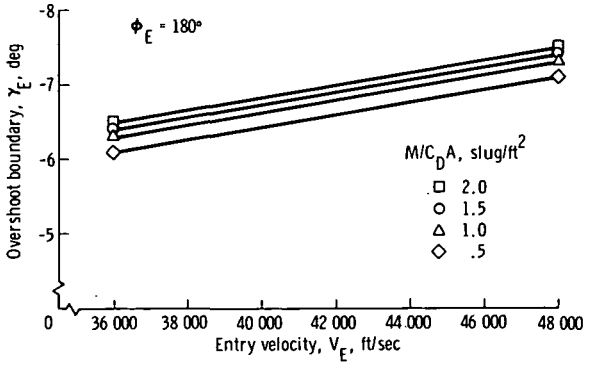


(b) L/D = 0.25.

Figure 26.- Overshoot boundary entry-flight-path angle as a function of entry velocity.

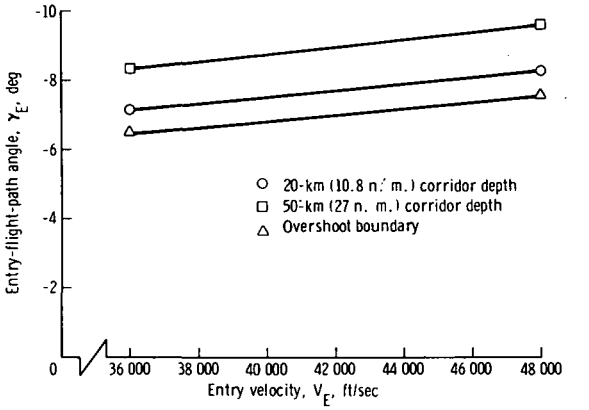


(a) L/D = 0, M/$C_D$A = 0.5 slug/ft$^2$.

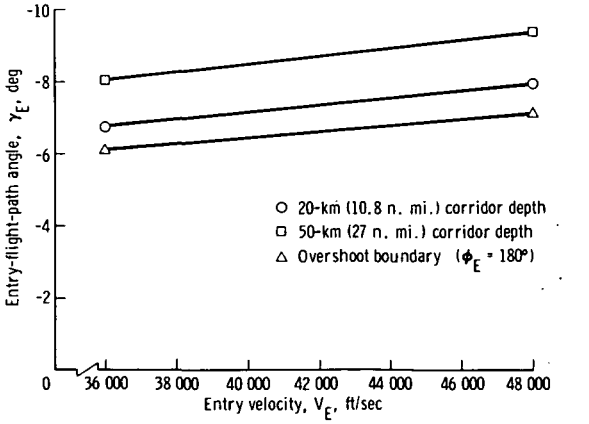


(b) L/D = 0.25, M/$C_D$A = 0.5 slug/ft$^2$.

Figure 27.- Entry-flight-path angle as a function of entry velocity for the overshoot boundary, the 10.8-n. mi. entry corridor, and the 27-n. mi. entry corridor.

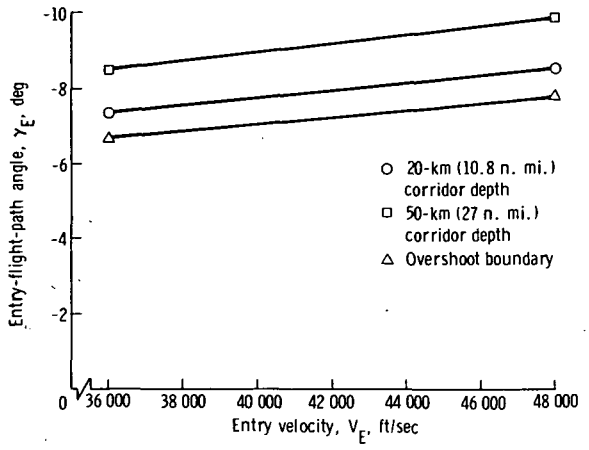


(c) L/D = 0, $M/C_DA$ = 1.0 slug/ft$^2$.

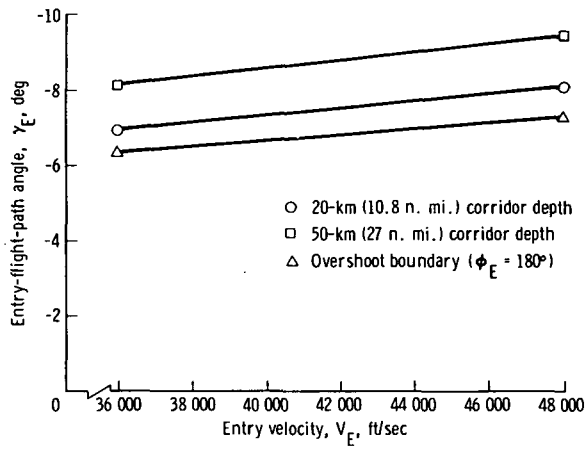


(d) L/D = 0.25, $M/C_DA$ = 1.0 slug/ft$^2$.

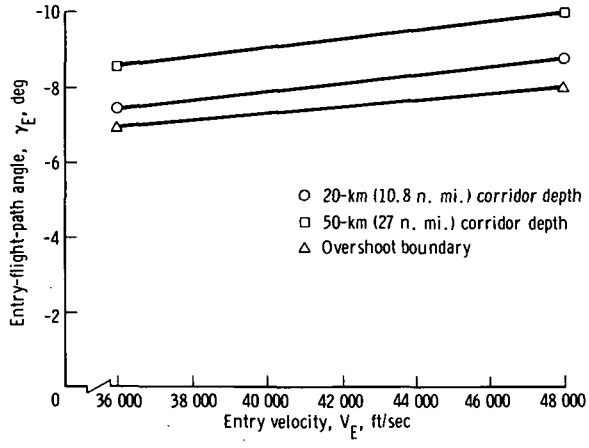


(e) L/D = 0, $M/C_DA$ = 1.5 slug/ft$^2$.

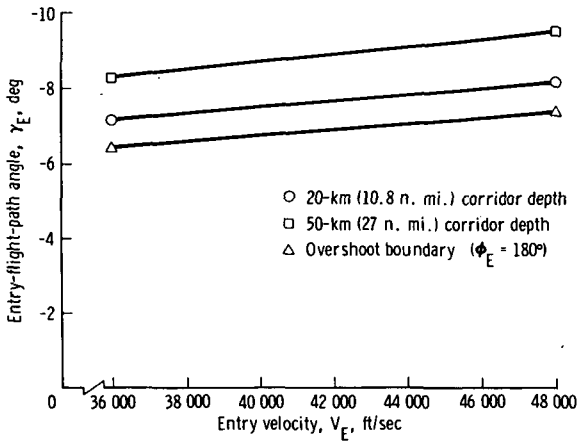


(f) L/D = 0.25, $M/C_DA$ = 1.5 slug/ft$^2$.

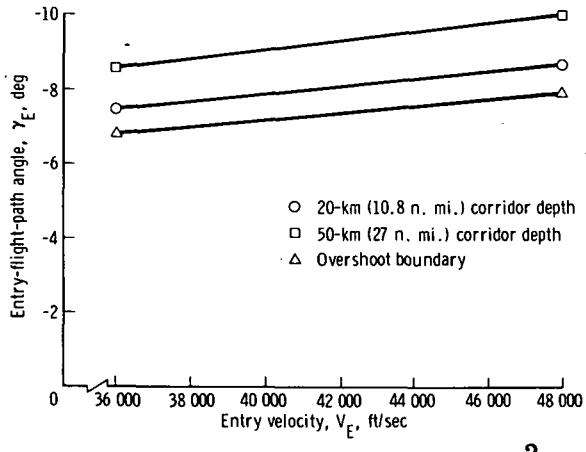


(g) L/D = 0, $M/C_DA$ = 2.0 slug/ft$^2$.

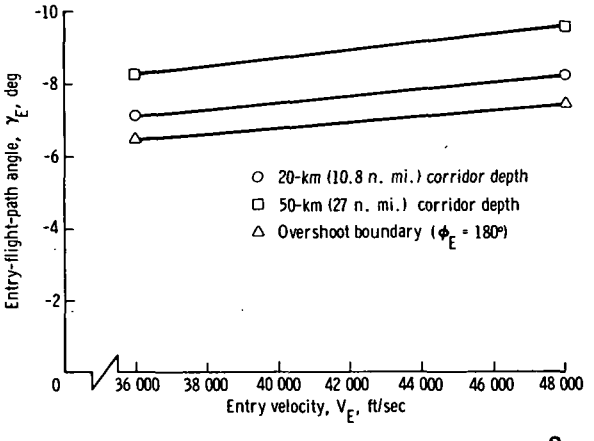


(h) L/D = 0.25, $M/C_DA$ = 2.0 slug/ft$^2$.

Figure 27.- Concluded.

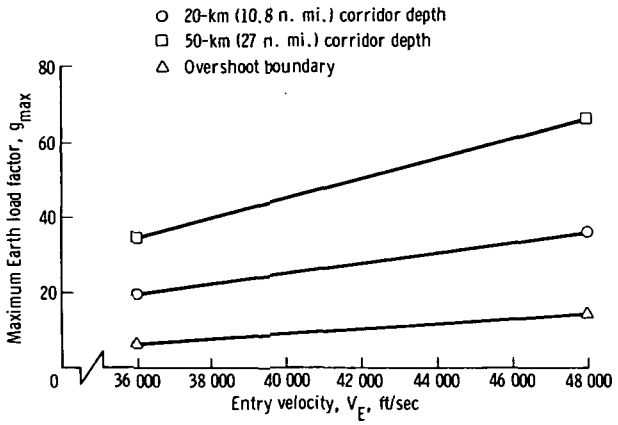


(a) $L/D = 0$, $M/C_DA = 0.5$ slug/ft$^2$.

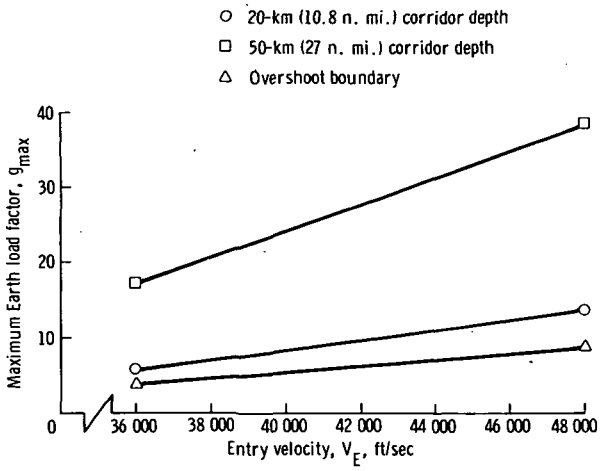


(b) $L/D = 0.25$, $M/C_DA = 0.5$ slug/ft$^2$.

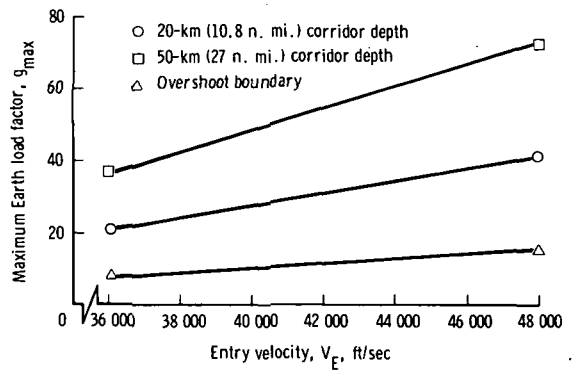


(c) $L/D = 0$, $M/C_DA = 1.0$ slug/ft$^2$.

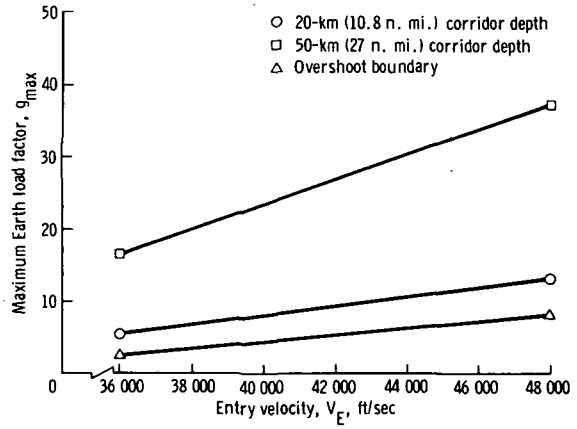


(d) $L/D = 0.25$, $M/C_DA = 1.0$ slug/ft$^2$.

Figure 28.- Maximum Earth load factor as a function of entry velocity for the overshoot boundary, the 10.8-n. mi. entry corridor, and the 27-n. mi. entry corridor.

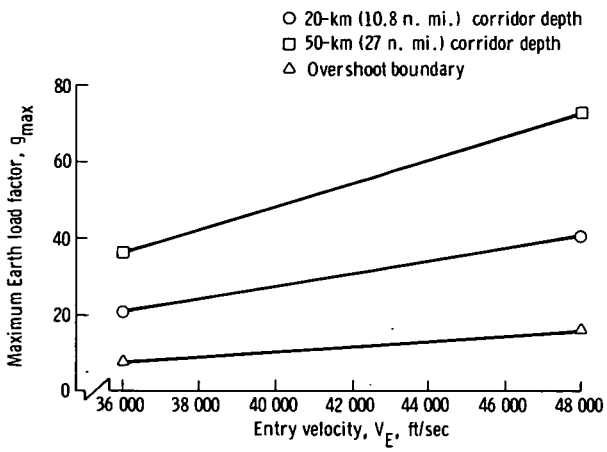


(e) L/D = 0, $M/C_DA$ = 1.5 slug/ft$^2$.

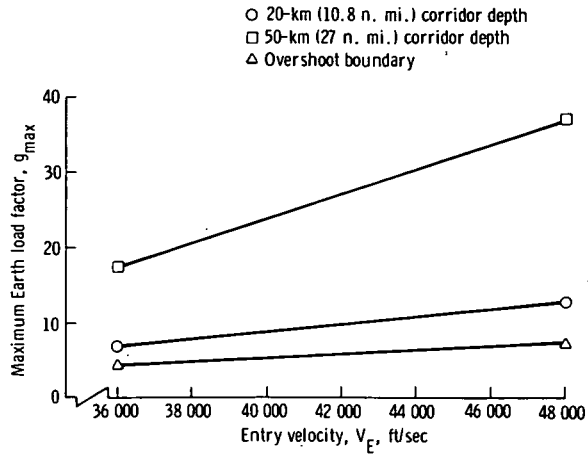


(f) L/D = 0.25, $M/C_DA$ = 1.5 slug/ft$^2$.

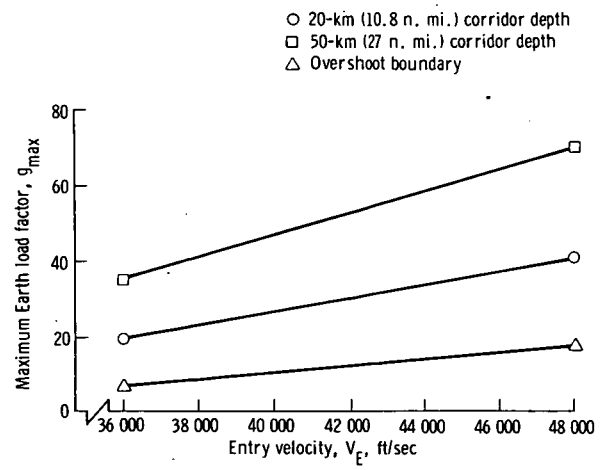


(g) L/D = 0, $M/C_DA$ = 2.0 slug/ft$^2$.

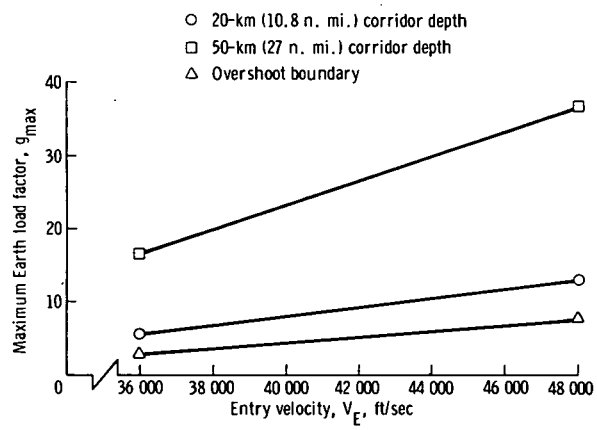


(h) L/D = 0.25, $M/C_DA$ = 2.0 slug/ft$^2$.

Figure 28.- Concluded.

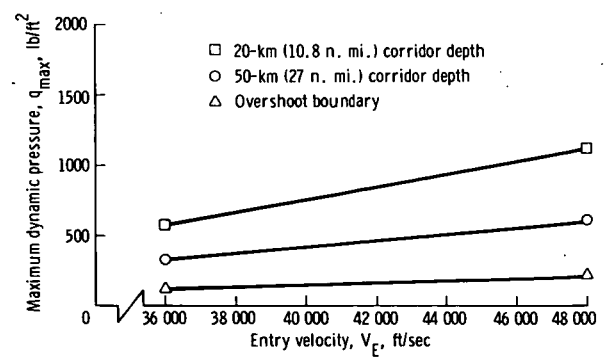


(a) L/D = 0, $M/C_DA$ = 0.5 slug/ft$^2$.

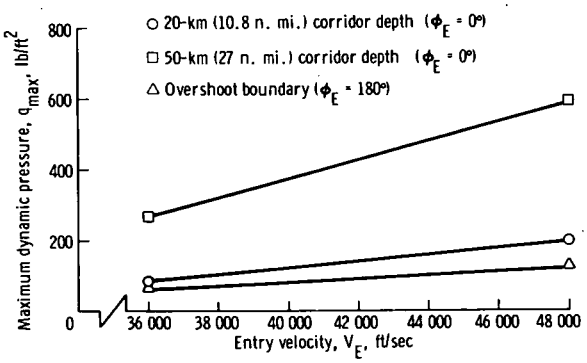


(b) L/D = 0.25, $M/C_DA$ = 0.5 slug/ft$^2$.

Figure 29.- Maximum dynamic pressure as a function of entry velocity for the overshoot boundary, the 10.8-n. mi. entry corridor, and the 27-n. mi. entry corridor.

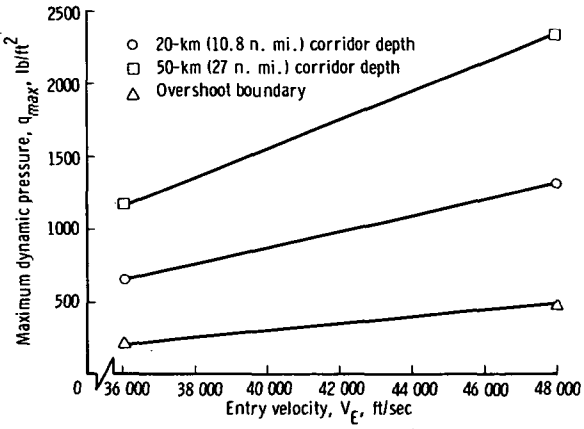


(c) L/D = 0, $M/C_DA$ = 1.0 slug/ft$^2$.

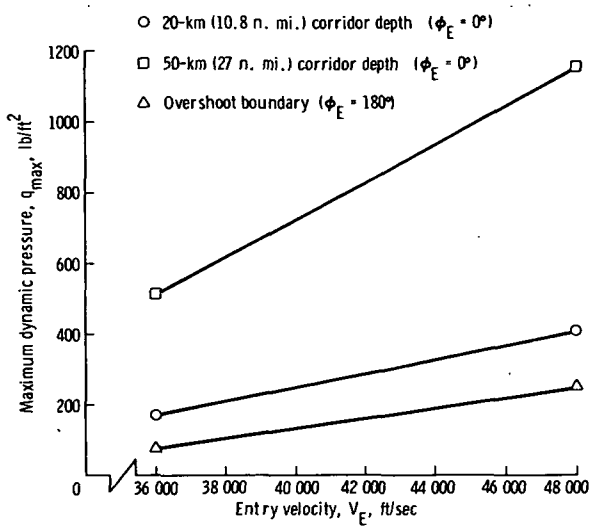


(d) L/D = 0.25, $M/C_DA$ = 1.0 slug/ft$^2$.

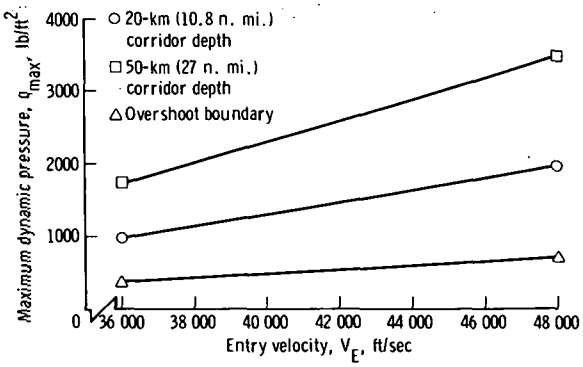


(e) L/D = 0, $M/C_DA$ = 1.5 slug/ft$^2$.

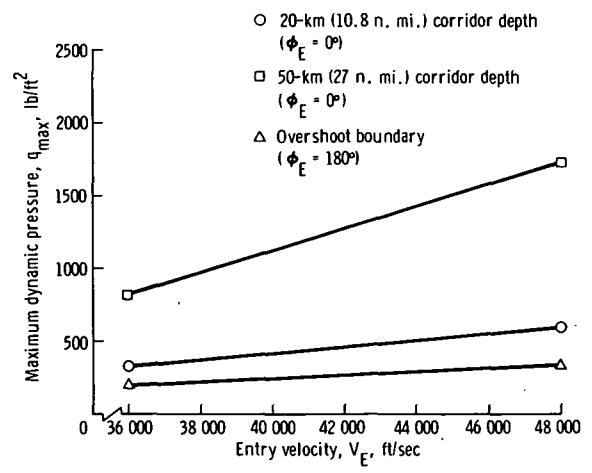


(f) L/D = 0.25, $M/C_DA$ = 1.5 slug/ft$^2$.

Figure 29. - Continued.

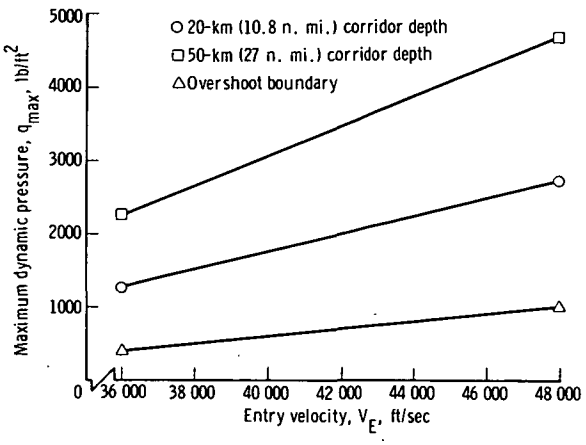


(g) L/D = 0, $M/C_DA$ = 2.0 slug/ft$^2$.

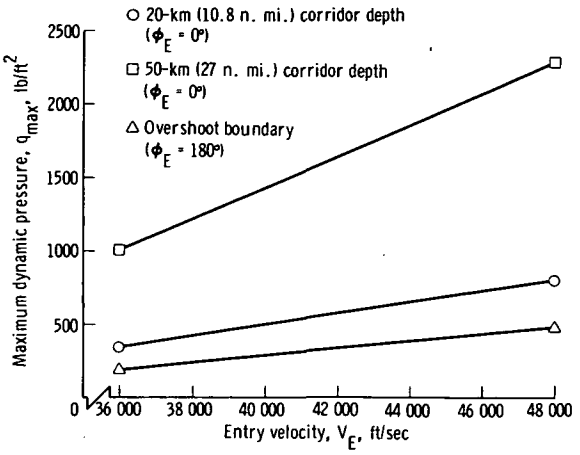


(h) L/D = 0.25, $M/C_DA$ = 2.0 slug/ft$^2$.

Figure 29.- Concluded.

Flight-performance characteristics for entry-from-orbit operations are presented in figures 30 to 34. The overshoot boundary entry-flight-path angle is shown to be slightly dependent on the spacecraft ballistic parameter for entry velocities of 24 000 and 30 000 ft/sec (fig. 30). The overshoot boundary vacuum periapsis radius as a function of the spacecraft ballistic parameter is presented in figure 31.

The entry velocity and entry-flight-path angle are presented as a function of the apoapsis retrofire velocity reduction for the typical case of deorbit from a 200- by

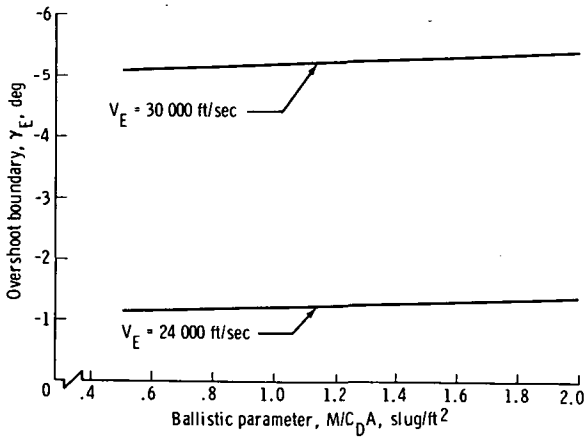


(a) L/D = 0.

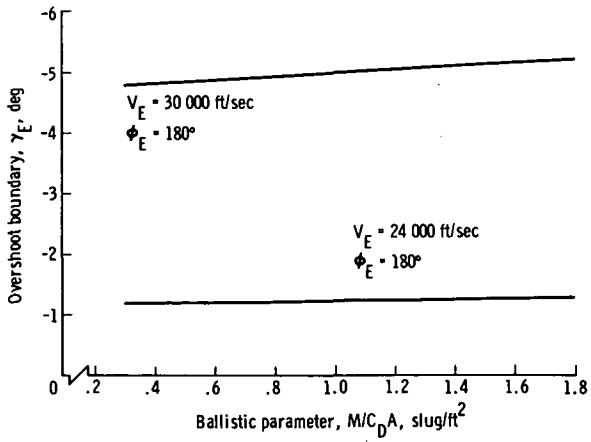


(b) L/D = 0.25.

Figure 30.- Entry-from-orbit overshoot boundary flight-path angle as a function of spacecraft ballistic parameter.

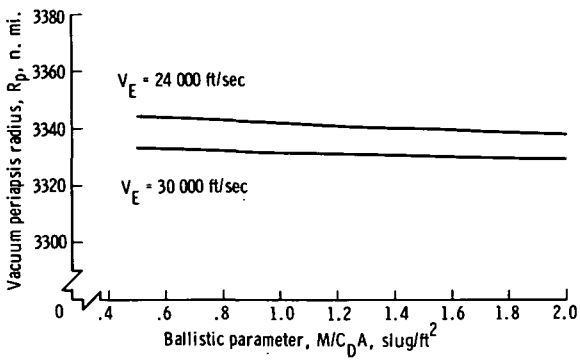


(a) L/D = 0.

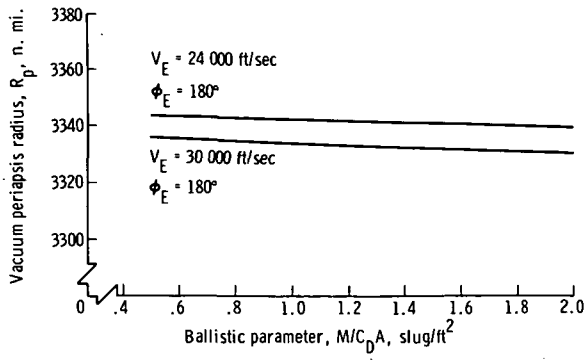


(b) L/D = 0.25.

Figure 31.- Entry-from-orbit overshoot boundary vacuum periapsis radius as a function of spacecraft ballistic parameter.

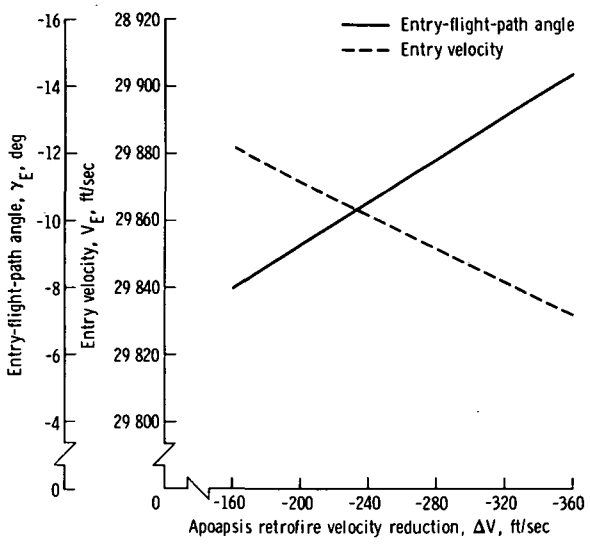


Figure 32.- Entry-flight-path angle and velocity as a function of apoapsis retrofire velocity reduction for deorbit from a 200- by 10 000-n. mi. elliptical orbit.

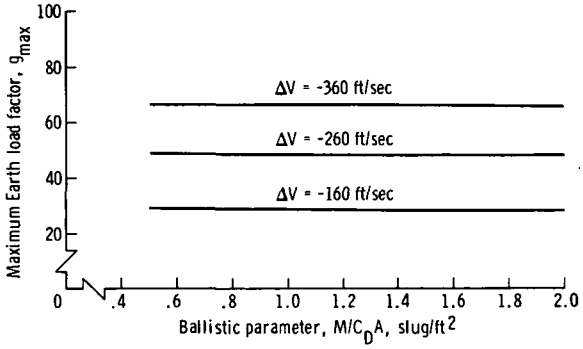


Figure 33.- Maximum Earth load factor as a function of spacecraft ballistic parameter for entry from a 200- by 10 000-n. mi. elliptical orbit; L/D = 0.

10 000-n. mi. elliptical parking orbit (fig. 32). Maximum Earth load factors for such deorbits are dependent on values of the apoapsis velocity reduction rather than the spacecraft ballistic parameter (fig. 33). The maximum dynamic pressure associated with these deorbits, although dependent on the apoapsis velocity reduction, is also dependent on the spacecraft ballistic parameter. An increase in the ballistic parameter increases the associated dynamic pressure for a given apoapsis velocity reduction value (fig. 34).

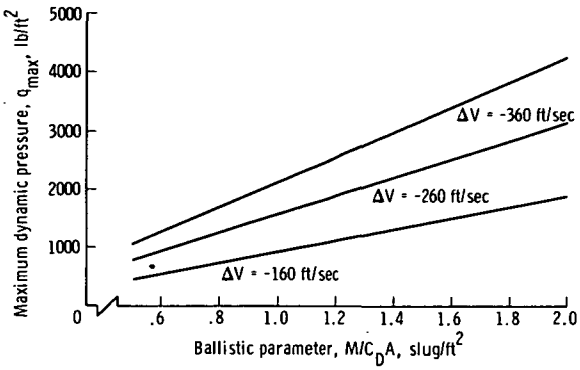


(a) L/D = 0.

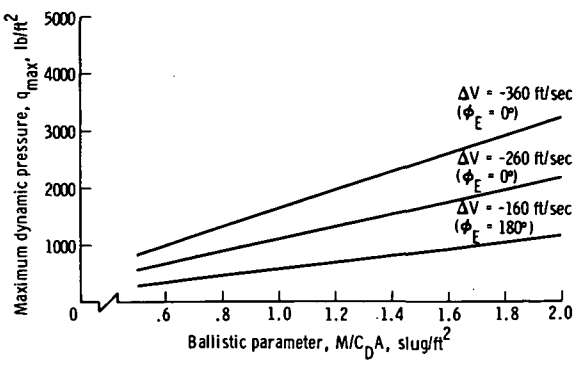


(b) L/D = 0.25.

Figure 34.- Maximum dynamic pressure as a function of spacecraft ballistic parameter for entry from a 200- by 10 000-n. mi. elliptical orbit.

## CONCLUDING REMARKS

An analysis has been completed to show the effects of both spacecraft and trajectory characteristics on entry performance into a proposed atmosphere of Venus. This atmosphere was derived from data obtained by the Mariner V and the Venera IV spacecraft. Consideration was given to both manned and unmanned missions. A general review of design-parameter trending information gained from the quantitative data of the analysis would include (for the manned vehicle entry) the following facts.

1. The corridor depth is insensitive to variance in the spacecraft ballistic parameter.

2. An increase in the spacecraft ballistic parameter lowers the pullout altitude but does not affect the pullout velocity appreciably.

3. The entry-corridor depth is reduced by an increase in the entry velocity.

4. An increase in entry velocity increases the pullout altitude associated with the undershoot boundary but decreases the pullout altitude associated with the overshoot boundary.

5. An increase in the spacecraft lift-to-drag ratio capability increases the entry-corridor depth.

6. The maximum dynamic pressure encountered by an entry vehicle is decreased by increasing the vehicle lift-to-drag.

7. A ±50 percent atmospheric-density deviation reduces the entry-corridor depth by approximately 3.5 n. mi. for a vehicle of lift-to-drag ratio of 0.5 and by 3.0 n. mi. for a vehicle lift-to-drag ratio of 1.0. These reductions are a function of only the spacecraft lift-to-drag ratio and do not vary appreciably over the range of ballistic parameters or entry velocities that were considered.

Design trending data for unmanned vehicle entry would include the following factors.

1. An increase in spacecraft ballistic parameter increases the entry angle associated with the overshoot boundary.

2. An increase in the spacecraft ballistic parameter increases the maximum dynamic pressure encountered during entry but does not affect appreciably the maximum deceleration loads over the given range of parameters.

3. Increasing the entry velocity increases the overshoot boundary entry angle and the maximum dynamic pressure and maximum deceleration loads encountered during entry.

4. An increase in the deorbit apoapsis retrofire velocity reduction increases the associated atmospheric entry angle while decreasing the entry velocity.

5. An increase in probe lift-to-drag capability from 0 to 0.25 decreases the maximum dynamic pressure and maximum deceleration loads by approximately one half.

Manned Spacecraft Center
National Aeronautics and Space Administration
Houston, Texas, December 28, 1972
976-30-90-01-72

# REFERENCES


1. Dennison, A. J.; and Butler, J. F.: Missile and Satellite Systems Program for the IBM 7090. Technical Information Serial 61 SD 170, Missile and Space Vehicle Dept., General Electric Co., Feb. 1962.

2. Chapman, D. R.: An Approximate Analytical Method for Studying Entry Into Planetary Atmospheres. NASA TR R-11, 1959.

3. Chapman, D. R.: An Analysis of the Corridor and Guidance Requirements for Supercircular Entry Into Planetary Atmospheres. NASA TR R-55, 1960.

4. Allen, H. J.; and Eggers, A. J.: A Study of the Motion and Aerodynamic Heating of Ballistic Missiles Entering the Earth's Atmosphere at High Supersonic Speed. NACA Rep. 1381, 1958.

5. Evans, D. E.; Pitts, D. E.; and Kraus, G. L.: Venus and Mars Nominal Natural Environment for Advanced Manned Interplanetary Mission Programs. NASA SP-3016, 1967.

6. Koenig, L. R.; Murray, F. W.; Michaux, C. M.; and Hyatt, H. A.: Handbook of the Physical Properties of the Planet Venus. NASA SP-3029, 1967.

7. Owen, R. B.; Hasseltine, C. L.; Roberts, W. T.; West, G. S.; and Scissum, J. A.: The Environment of Venus: A Discussion of its Atmosphere and Surface. NASA TM X-53497, 1967.

8. Kliore, A.; and Cain, D. L.: Mariner 5 and the Radius of Venus. Journal of Atmospheric Sciences, vol. 25, July 1968, pp. 549-553.

9. Tass: Pravda, No. 295, Oct. 22, 1967, pp. 6-7.

10. Tass: Izvestia, No. 257, Oct. 31, 1967.

11. Reese, D. E.; and Swan, P. R.: Venera 4 Probes Atmosphere of Venus. Science, vol. 159, Mar. 15, 1968, pp. 1228-1230.

12. Ash, M. E.; Shapiro, I. I.; and Smith, W. P.: Astronomical Constants and Planetary Ephemerides Deduced from Radar and Optical Observations. Astron. J., vol. 72, no. 3, 1967, pp. 338-350.

13. Melbourne, W. G.; Muhleman, D. O.; and O'Handley, D. A.: Radar Determination of the Radius of Venus. Science, vol. 160, May 31, 1968, pp. 987-988.

14. Wingrove, R. C.: Trajectory Control Problems in Planetary Entry of Manned Vehicles. J. Spacecraft Rockets, vol. 2, no. 6, Nov.-Dec. 1965, pp. 883-888.

15. Murtagh, T. B.: Planetary Probe Guidance Accuracy Influence Factors for Conjunction-Class Missions. NASA TN D-4852, 1969.

16. Repic, E. M.; Boobar, M. G.; and Chapel, F. G.: Aerobraking as a Potential Planetary Capture Mode. J. Spacecraft Rockets, vol. 5, no. 8, Aug. 1968, pp. 921-926.